RICE UNIVERSITY

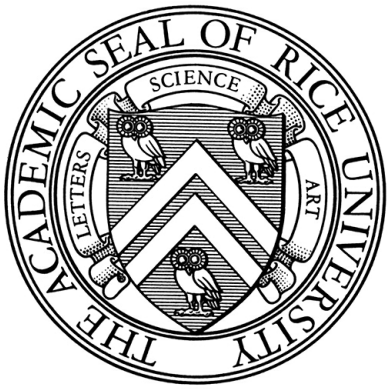

ELECTRON PHASE COHERENCE IN MESOSCOPIC NORMAL METAL WIRES

by

Aaron James Trionfi

DOCTOR OF PHILOSOPHY

HOUSTON, TEXAS

November, 2006

RICE UNIVERSITY

Electron Phase Coherence in Mesoscopic Normal Metal Wires

by

Aaron James Trionfi

A THESIS SUBMITTED
IN PARTIAL FULFILLMENT OF THE
REQUIREMENTS FOR THE DEGREE

Doctor of Philosophy

APPROVED, THESIS COMMITTEE:

Douglas Natelson, Chair
Associate Professor of Physics and Astronomy
and Electrical and Computer Engineering

Peter Nordlander
Professor of Physics and Astronomy

Kevin Kelly
Assistant Professor of Electrical
and Computer Engineering

HOUSTON, TEXAS
November, 2006

Abstract

ELECTRON PHASE COHERENCE IN MESOSCOPIC NORMAL METAL WIRES

by

Aaron James Trionfi

Corrections to the classically predicted electrical conductivity in normal metals arise due to the quantum mechanical properties of the conduction electrons. These corrections provide multiple experimental tests of the conduction electrons' quantum phase coherence. I consider if independent measurements of the phase coherence via different corrections are quantitatively consistent, particularly in systems with spin-orbit or magnetic impurity scattering. More precisely, do independent quantum corrections to the classically predicted conductivity depend identically on the ubiquitous dephasing mechanisms in normal metals? I have inferred the coherence lengths from the weak localization magnetoresistance, magnetic field-dependence of time-dependent universal conductance fluctuations, and magnetic field-dependent universal conductance fluctuations, three observable quantum corrections, in quasi one- and two-dimensional AuPd wires and quasi-1D Ag and Au wires between 2 and 20 K. While the coherence lengths inferred from weak localization and time-dependent universal conductance fluctuations are in excellent quantitative agreement in AuPd, the strong quantitative agreement is apparently lost below a critical temperature in both Ag and Au. Such a disagreement is inconsistent with current theory and must be explained. I developed a hypothesis attributing the coherence length discrepancy seen in Ag and Au to a crossover from the saturated to unsaturated time-dependent conductance fluctuation regime. Two experimental tests were then employed to test this hypothesis. One test examined the effects of a changing spin-flip scattering rate in Au while the second examined how passivation of the two level systems responsible for time-dependent conductance fluctuations at the surface of a Au nanowire affects the inferred coherence lengths. The results of the two tests strongly indicate that the observed disagreement in Au (and likely Ag) is indeed due to a crossover from saturated to unsaturated time-dependent conductance fluctuations.

Acknowledgments

During my graduate student orientation five years ago, then university president Malcolm Gillis promised that the time I spent at Rice would be a time of great intellectual advancement. Dr. Gillis could not have been more correct. The bulk of the knowledge I acquired here can be directly attributed to the outstanding guidance of my advisor Dr. Doug Natelson. He has found an amazing balance to stay closely connected with the day-to-day activities of his students without simultaneously micromanaging. He truly gave me the guidance I needed while still allowing me to err, learn, and discover on my own. Without this help I would certainly still be toiling away in lab. A short paragraph is not nearly enough words to express my gratitude for Doug's direction, advice, but most importantly his faith in my ability to do "good science."

I would like to thank my committee members, Dr. Kevin Kelly and Dr. Peter Nordlander, for volunteering their time to read this thesis and hear my defense. Their questions and comments certainly helped improve my thesis.

Much like any group environment, a lab is what the scientists make of it. That said, I cannot thank my fellow graduate students enough for always making the Natelson lab a wonderful place to learn and work. Lam Yu, the senior student for much of my time here, was always willing to show me how to use the various equipment and teach me some of the more useful aspects of Labview coding. I would like to thank Behrang Hamadani for all the hours we spent working out difficult homework problems and all the interesting conversations he would strike up with me. Sungbae Lee was especially helpful with the work in this thesis. He was always ready to perform an experiment for me if I was traveling or just unable to make it to lab. I would also like to thank him for all the great rounds of golf we played together. I would like to thank Zach Keane for his constant reminders about how few people actually cared about my work, and his frequent requests that I die in a fire. His dry sense of humor added another enjoyable personality that left few dull moments in lab. Finally, I would like to thank the newest additions to the lab, Dan Ward and Jeff Worne. They have taken my good-natured ribbing as it was intended, and I am certainly glad for that. Getting to know each of them for the last year has left little doubt that as all the senior students of our lab leave, the Natelson lab will be left in very capable hands.

I would also like to acknowledge the support of all my family and friends. My

good friend Kevin Sims has been like a brother to me since high school and no distance has ever seemed to diminish our friendship. My friend and roommate Andrew Osgood. I have never had a roommate easier to get along with. Sharing an apartment for the last three years was certainly one of the best decisions I made while in Houston. I would like to thank all my uncles and aunts for their support regardless of what I was doing. Not seeing them more regularly was definitely one of the hardest parts of graduate school. I would like to thank both my grandmothers, Bubbie and Baba. I am grateful for the unconditional love and support both have given me throughout my life. All the cookies, cakes, and other goodies they always had waiting for me didn't hurt either. I would also like to thank my grandfather; I called him Papa. He passed away while I was finishing college, but the lessons he taught me may be the most important of all. His appreciation of family and the time spent with them was instilled in me from an early age. That is a lesson I will never allow myself to forget.

Finally, my immediate family. My twin brother Jonathon, who was both my best friend and my arch nemesis. The competition between us almost always led to success for both of us (as well as some incredible fights). Not having him around to hang out with all the time has taken quite a while to get accustomed to (I am almost there). And finally, my parents, Frank and Sue. I cannot begin to list all the reasons I need to thank them both so I will just pick a few. Their decision to involve me in childhood activities like sports and cub scouts has given me countless fond memories and life lessons. Their commitment to my education and encouragement never wavered; they always stressed the importance of school and rewarded my successes, but never demanded anything more than my best effort in my studies. Most of all, though, I wish to thank them for their willingness to keep an open mind when I told them I was studying physics. Although neither had any familiarity with the subject, instead of criticizing my decision they went and researched the future prospects of a person with a degree in physics. After learning that I, indeed, could find a job with such a degree, they were in full support of my decision (no doubt they would have supported me regardless of what their research uncovered).

Table of Contents

List of Figures

Chapter 1

Introduction

1.1 Background

1.1.1 Introduction

An important goal of condensed matter physics in the last century has been the understanding of electrical conduction in metals. The pursuit of a quantitative understanding of this topic has led scores of theoretical and experimental physicists through classical statistics, quantum mechanics, and field theory. The models attempting to explain observed effects have become more and more complex. The initial theory of electrical transport, namely the Drude model, and the corrections to this theory are an enormous topic that could not possibly be completely explained in these pages. The perturbative corrections to the Drude model due to the quantum mechanical nature of the electron are collectively known as quantum transport phenomena (QTP) and are the focus of this paper. Other corrections to the Drude model involve incorporating the effects due to interactions of the electrons with both the ionic lattice and other electrons in the metal. The most common example is the band structure of metals. Without incorporating the lattice potential into the analysis of electron conduction, this behavior is completely unexplainable. It should also be pointed out that quantum transport phenomena are not always the only important correction to the classical conductivity, even in mesoscopic systems. For instance, two effects widely studied in mesoscopic physics, the Quantum Hall Effect and Coulomb Blockade in quantum dots, are dominated by electron-electron interactions. A review of

both the Drude model and the basic theories of three quantum transport phenomena: the magnetic Aharonov-Bohm effect (AB effect), Weak Localization (WL), and Universal Conductance Fluctuations (UCF), will be covered.

The theories explaining much of the phenomena discussed in this paper have been well understood for at least twenty years. In spite of this fact, there are still many people exploring the topic. It is fair to conclude that unanswered questions within the field must remain. One important question is whether the relevant length scales of these various phenomena are the same. Said another way, "Do the ubiquitous dephasing mechanisms in a normal metal influence all the quantum transport phenomena in precisely the same manner?" The other question of great importance is the origin of the saturation of these effects at very low temperatures. The answer to these two questions are still not completely clear as will be seen later. The work presented in the following pages will attempt to answer the first question.

The understanding of how the quantum behavior of electrons changes in different environments is also extremely important as the search for a solid-state quantum computer continues. As will be discussed extensively, quantum transport phenomena give experimentalists a powerful tool to probe electron phase coherence and the mechanisms in metals that lead to electronic decoherence. A firm understanding of these mechanisms and the limitations they introduce are sure to influence whether a solid-state quantum computer is feasible.

1.1.2 Historical Perspective

A previous attempt to determine whether the same coherence physics is responsible for the behavior of time-dependent (TD) UCF and WL in quasi-2D Ag thin films resulted in equivocal results [1]. The test showed that above a critical temperature, the two phenomena were dominated by precisely the same dephasing mechanisms, but below the critical temperature the WL and TDUCF seemed to be controlled by different dephasing rates. The main result of this work is shown in Figure 1.1. At the time these findings were published, the results were consistent with accepted theory. The theoretical prediction stated the pertinent dephasing rate in WL was determined by Nyquist scattering (electron-electron scattering) while TDUCF were dominated by something called the out-scattering rate [2]. The out-scattering rate is simply defined as the rate at which an electron will change its momentum state in the Boltzmann formalism.

For roughly 3 years the results of the Ag comparison needed no further exploration due to their strong agreement with theoretical predictions. However, in 2002 a new theoretical treatment showed that although the out-scattering and Nyquist rates are indeed different under certain conditions, the important dephasing rates for both WL and UCF should be identical [3]. The Ag findings, thus, required an explanation. The only suggestion was that a subtle effect due to spin-orbit scattering was the cause of the discrepancy. We decided to revisit this problem in a series of tests with Ag, Au, and a AuPd alloy. Due to the stronger spin-orbit scattering in AuPd and Au, the hypothesis that spin-orbit coupling is the cause of the previous Ag results can be tested.

Although it will not be a main point of this thesis, the issue of coherence saturation

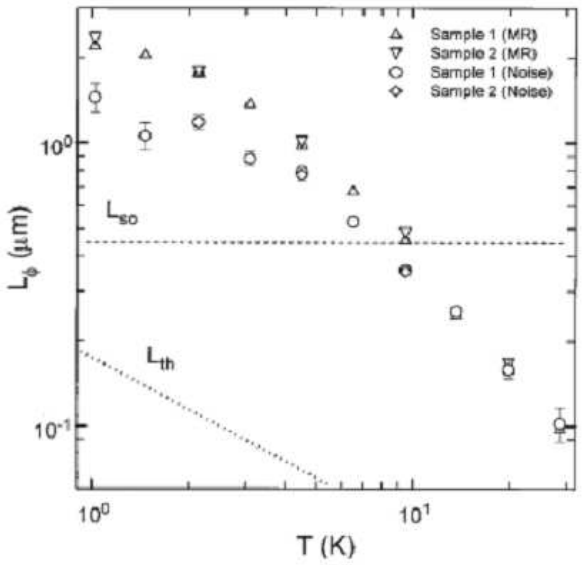

Figure 1.1: The coherence lengths from two quasi-2D Ag films. The coherence lengths were inferred from weak localization magnetoresistance curves and the field dependence of time-dependent universal conductance fluctuations. Data from [1].

bears mentioning. In 1997, results were published showing that below a critical temperature, the dephasing rate stopped decreasing [4]. Theoretically the dephasing rate should go to zero as the temperature approaches zero. A controversial hypothesis suggested by the authors of [4] states that zero-point fluctuations of the electrons cause an intrinsic dephasing mechanism leading the dephasing rate to become temperature independent as the temperature approaches zero. Yet another group suggests the perturbative treatment of the electron-electron interactions leading to a vanishing dephasing rate as the temperature goes to zero fails to treat long time scale interactions [5]. These two hypotheses started a still-ongoing debate as to the cause of coherence saturation. One camp has accepted that the observed dephasing is intrinsic while the other camp has argued that external dephasing mechanisms are the culprit [6, 7].

As the coherence saturation debate continues, arguments from both sides have attempted to compare results from different quantum transport phenomena. Without understanding whether these phenomena are truly controlled by the same length scales, it would appear unwise to try and compare the coherence lengths inferred from two different QTP.

1.2 Classical Transport

1.2.1 Electrical Conductivity

The logical beginning to a discussion of electrical conductivity is a statement of Ohm's Law. For use in the following discussion, Ohm's Law will be written in terms of the electric field and current density.

$$\vec{j} = \sigma \cdot \vec{E} \tag{1.2.1}$$

The constant σ is known as the conductivity of the material. For the purposes of this paper equation 1.2.1 is adequate, but the most general form of Ohm's law must have a conductivity tensor rather than a constant. This tensor arises due to current densities that are not parallel to the applied field.

In 1900, P. Drude presented his theory of electrical conduction [8] based upon the ideas developed in the Kinetic Theory of Gases. He assumed that the charge carriers in a metal were free particles that experienced collisions while propagating. One of the key aspects of the Kinetic Theory is that the particles do not interact except for the moment they collide. The idea of charge carriers experiencing collisions is fundamentally correct with a few subtle problems. Kinetic Theory treats the result of each collision as a randomization of the particle's momentum with no influence due to previous collisions.

This idea of an uncorrelated interaction (with previous interactions) is known as a Markov Process. As will be seen later, this assumption cannot be used to explain all the effects seen in electrical transport. Another problem is that electrons are charged particles and, thus, do interact via the electric fields produced by each electron. The interaction between an electron and the electric field produced by all the other electrons is, in fact, the main dephasing mechanism in many systems. The last issue that will be important is how electrons interact with the positively charged ion cores. The Bloch theorem explains that an electron will only scatter off such an ion core if it has somehow broken the periodicity of the ion lattice. This idea will be important when explaining electron motion in a disordered metal. A review of Drude's theory can be explored, with the understanding that the following derivation must be corrected later.

The theory starts with a known conduction electron density, n, within a metal. If these electrons move collectively with a speed v, then the current density within the metal can be written as:

$$\vec{j} = -ne\vec{v} \tag{1.2.2}$$

However, all the electrons in a metal do not move collectively. Electrons are moving randomly throughout the metal with an average velocity of zero in the absence of a potential gradient. Once an electric field is applied, the electrons accelerate in response to the applied field. If the field is constant, then using Newton's Second Law and the Lorentz force gives a velocity:

$$\vec{v} = \vec{v}_0 - e\vec{E}t \tag{1.2.3}$$

Taking the average velocity of all the electrons eliminates $\vec{v}_0$ while the second term is just

the average time between collisions multiplied by the constant in front of t. τ is known as the relaxation time and is the average time between collisions. Plugging the average velocity back into equation 1.2.2 gives a current density of:

$$\vec{j} = \left(\frac{ne^2\tau}{m}\right)\vec{E} \tag{1.2.4}$$

Comparing equation 1.2.4 with equation 1.2.1, a conductivity of $\frac{ne^2\tau}{m}$ is recovered. This is typically referred to as the Drude conductivity [9].

1.2.2 Diffusive Motion

One last topic that needs review is the idea of diffusive motion. The Drude model above uses the average velocity to find a current in a wire. This treatment accomplishes its goal, but leaves out the explanation of how an electron actually moves through a wire. The relaxation time, τ, accounts for the motion of the electron in this theory. In general, if an electron travels for longer than the relaxation time, then the length the electron travels will not be the velocity multiplied by the time. Since multiple collisions occur, the electron's path is quite complicated. This is known as diffusive motion (the idea is sometimes called a random walk). In this case, the important quantity is not the velocity of the electron, but the diffusion constant of the metal. If an electron travels for time t through a metal with diffusion constant D, then the length it traveled on average is:

$$L = \sqrt{Dt} \tag{1.2.5}$$

The diffusion constant of a metal can be calculated if the mean free path and Fermi velocity of the metal are known. The relation is:

$$D = \frac{1}{d}v_{\mathrm{f}}l \tag{1.2.6}$$

The value d is the dimensionality of the metal for diffusive motion. Equation 1.2.5 will be used extensively to relate time and length in later discussions. If the dimensions of the metal are all greater than the mean free path of the electron, then d will be equal to three.

1.3 Quantum Transport

1.3.1 Introduction

Although electrical conduction through a metal in macroscopic samples at room temperature can be explained very well treating charge carriers as classical free particles, all conduction phenomena cannot be explained with the Drude model. The reason is that charge carriers in metals (electrons) are not classical, non-interacting entities. Thus, one would expect corrections to the Drude conductivity due to, among others, quantum effects. As mentioned earlier, these corrections are known as quantum transport phenomena. They come about due to the phase of the electron's wave function and how this phase changes as the electron propagates through a metal. A quick review of quantum interference will lead to the first, and most transparent, of these phenomena, the magnetic Aharonov-Bohm effect.

Although the work presented in the pages of this thesis does not deal with the observation of the Aharonov-Bohm effect, the explanation of the phenomenon provides a great deal of insight into the theory explaining the phenomena of interest, Weak Localization and Universal Conductance Fluctuation Theory.

1.3.2 Quantum Interference

Consider a free electron with partial wave functions $\psi_{\mathrm{j}}(\vec{x}) = A_{\mathrm{j}}(\vec{x})e^{i\phi_{\mathrm{j}}}$ where j represents each possible path the electron can take through the metal and $\vec{x} = 0$ is the initial position of the electron. Feynman explained that to treat a quantum mechanical particle's propagation, each possible path must be considered, thus each partial wave function needs to be included in any probability calculation [10]. Therefore, the probability of the electron to be at any point $\overrightarrow{x}$ is:

$$P(\vec{x}) = \left| \sum_{\mathrm{j}} A_{\mathrm{j}}(\vec{x})e^{i\phi_{\mathrm{j}}} \right|^2 \tag{1.3.1}$$

The absolute value squared in the probability leads to cross terms that can be thought of as interference terms since only these terms will depend on the phase of each path. This is identical to the interference seen in optical phenomena (the double slit experiment for example).

The simplest yet non-trivial example of this idea is when there are only two possible paths, 1 and 2. In this example equation 1.3.1 becomes:

$$P(\vec{x}) = |A_1|^2 + |A_2|^2 + 2|A_1^* A_2| \cos(\phi_1 - \phi_2) \tag{1.3.2}$$

As will be discussed shortly, the cosine term gives rise to the Aharonov-Bohm effect.

1.3.3 Electron Phase Coherence

Before continuing with a detailed explanation of the Aharonov-Bohm effect, it is necessary to discuss quantum coherence. The previous section laid the foundation of quantum interference, however, there is no discussion of the limitations of such interference. Just as in the optical case, in order for interference to occur, interacting waves must be phase

coherent. In the case of quantum interference, the interference is a result of a single particle and its partial wave functions. Therefore, initial phase coherence should be present between each path since they share the same value at $\vec{x} = 0$. However, whether each partial wave function will remain phase coherent after some length of its corresponding path is traversed is not as clear.

In order to determine how long an electron remains phase coherent, one must examine what affects the electron phase. Equation 1.3.3 shows the typical expression of the phase in a free electron.

$$\psi(\vec{x}) = A(\vec{x}) \exp[i(\vec{k} \cdot \vec{x} - Et/\hbar)] \tag{1.3.3}$$

From equation 1.3.3, it is clear that any position, momentum, or energy change of an electron will alter its phase. However, a simple phase change is not enough to cause dephasing. In order to cause dephasing, the wave function itself must no longer be an eigenstate of the system. Said another way, the partial wave function must become entangled with another degree of freedom. In classical mechanics, collisions involving extra degrees of freedom are inelastic. In many cases, it is inelastic collisions that are the sole source of phase decoherence in metals. In a disordered metal in the diffusive limit, a propagating electron will experience both elastic and inelastic collisions. With respect to quantum interference, however, it is the so-called inelastic mean free path or inelastic scattering length which will be the relevant length scale.

There are three different scattering processes that cause dephasing of conduction electrons: electron-electron interactions, electron-phonon interactions, and spin-flip interactions. The e-e and e-ph interactions each have a strong temperature dependence

while the strength of the spin-flip interactions is more strongly dependent on the concentration of impurities with a non-zero magnetic moment (the temperature dependence of the spin-flip scattering is small over the temperature range typically measured).

Electron-electron interactions can be thought of as a conduction electron being influenced by the electric field created by all the remaining conduction electrons. At finite temperatures, there exists a thermal energy, k_BT, which causes thermal fluctuations in the electronic density (later this will be referred to as Johnson noise). These fluctuations create an electric field that is, in turn, changed by the electron of interest. This interplay leads to electron dephasing. Since the cause of the fluctuating electric field is available thermal energy, the electron-electron dephasing rate decreases as the system temperature decreases. The actual temperature dependence is dependent on the system's dimension. For instance, the theoretical electron-electron dephasing rates for one and two-dimensional systems are [11]:

$$\tau_{\text{e-e}}^{-1} = \left(\frac{e^2\sqrt{2D}k_BTR}{\hbar^2 L}\right)^{2/3} \tag{1.3.4}$$

$$\tau_{\text{e-e}}^{-1} = k_BT\frac{e^2R_\square}{2\pi\hbar^2}\ln\left(\frac{\pi\hbar}{e^2R_\square}\right) \tag{1.3.5}$$

respectively. L is the wire length in equation 1.3.4 and $R_\square$ is the sheet resistance of the metal in equation 1.3.5.

Electron-phonon interactions are the scattering events that occur due to the breaking of the periodic symmetry that is present in the lattice potential. A consequence of Bloch's Theorem, a conduction electron in a Bloch state will not scatter from an ion as long as the ion is part of a lattice of periodic symmetry. Phonons (excited lattice vibration modes) lift such symmetry. A phonon may be treated as a quasi-particle that is

scattered by a conduction electron. Thus the collision is inelastic, resulting in dephasing of the conduction electron. Again, as the temperature decreases, the available phonons to absorb as well as the available phonon modes to emit into decreases resulting in a decreased dephasing rate.

Spin-flip interactions take place when extrinsic magnetic impurities are present in the system. Such impurities have magnetic moments creating a local magnetic field. As a conduction electron nears a magnetic impurity, its spin can couple to the local moment causing the spin to flip sign. The coupling entangles the spin and magnetic moment, and can result in dephasing. Clearly, the higher the density of magnetic impurities in the system, the more likely such spin-flip processes are to occur.

The total inelastic scattering length of the electron can be calculated using Matthiessen's Rule resulting in:

$$L_{\text{in}}^{-2} = L_{\text{e-e}}^{-2} + L_{\text{e-ph}}^{-2} + L_{\text{sf}}^{-2} \tag{1.3.6}$$

As will be seen later, the effect of spin-orbit scattering can also change the total coherence length of specific electrons. When this occurs, L_{in} and L_{ϕ} (the coherence length) are not equivalent and equation 1.3.6 must be corrected.

Not surprisingly, the coherence length also sets the dimensionality when discussing quantum transport phenomena. For instance, when a system has sides longer than the coherence length in all three dimensions, the system is considered three dimensional. Knowing the dimensionality of a system is very important when attempting to predict the behavior of all the quantum transport phenomena.

1.3.4 Aharonov-Bohm Phase

In order to experimentally observe the Aharonov-Bohm effect, a sample with two distinct coherent paths must be created that have a common origin and an intersection at some distance away from the origin such that neither path is greater than the coherence length. This is accomplished by making a circular sample with the source and drain leads attached to the circle to produce two equal semicircular paths. An example of such a sample is given in Figure 1.2 [7].

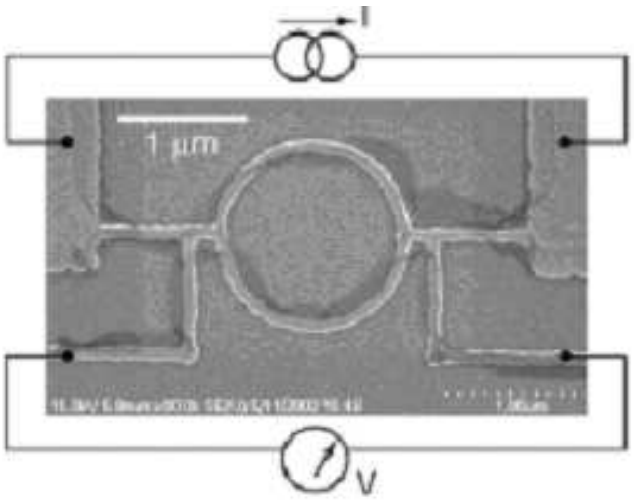

Figure 1.2: A copper Aharonov-Bohm ring. The source and drain have defined two distinct paths, one above and one below the two leads.

The fact that each semicircular path must be less than or equal to the coherence length of the electrons is a prime demonstration as to why mesoscopic systems are ideal for observing QTP. A typical L_ϕ in a normal metal wire at 300 K is about 1 nm while L_ϕ is about 1 μm at 2 K. Therefore, a mesoscopic metal wire cooled to about liquid helium temperatures provide ideal conditions for studying QTP.

It is important to note the system in Figure 1.2 actually contains many paths since the metal is in the diffusive regime. However, as long as the phase coherence is not lost while the electrons propagate from the source electrode to the drain, the Aharonov-Bohm effect should still be observable.

The conductivity of the sample in Figure 1.2 depends on the probability of each electron reaching the drain electrode, in other words the probability in equation 1.3.2. The conductivity should therefore oscillate with a changing phase difference between the two paths. To test this, a means of varying the phase difference between the two paths is necessary. A magnetic vector potential supplies such a means. The phase of an electron's wave function with respect to an azimuthal magnetic vector potential (a plane-perpendicular magnetic field) is given using the Peierls substitution resulting in the phase:

$$\phi = \phi_0 + \int \left(\overrightarrow{k} + \frac{e}{\hbar} \overrightarrow{A} \right) \cdot d\overrightarrow{l} \tag{1.3.7}$$

where $\overrightarrow{l}$ is the electron path and $\overrightarrow{A}$ is the magnetic vector potential. Applying equation 1.3.7 to each of the two semicircular paths, the phase difference is found to be:

$$\phi_1 - \phi_2 = \frac{eAB}{\hbar} \tag{1.3.8}$$

where A is the area of the ring and B is the applied field strength.

The phase difference in equation 1.3.8 is commonly referred to as the Aharonov-Bohm phase. Plugging equation 1.3.8 back into equation 1.3.2, the probability of an electron ending at the drain electrode is found to have an oscillating term with respect to the magnetic flux with a period of h/e. Therefore, an equivalent conductivity oscillation should be observed.

The fact that an electron's phase can be altered by a magnetic vector potential parallel to the electron's trajectory will be a recurring theme throughout the rest of this thesis. Thus, its importance in understanding the theories explaining WL and UCF cannot be understated.

1.4 This Thesis

The following thesis focuses on a quantitative comparison between coherence lengths inferred from two quantum transport phenomena, weak localization and time-dependent universal conductance fluctuations. Experiments were performed on three materials; gold, silver, and gold palladium alloy. The purpose of the tests were to determine the cause of a disagreement of coherence length information seen in an identical test of silver thin films. The following pages will explain both the basic theory of the phenomena as well as how each is experimentally observed and used to infer coherence information.

Chapter 2 will focus solely on weak localization. The chapter begins with a semi-classical derivation of the effect as well as a quasi-derivation of the effect a perpendicular magnetic field has on the phenomenon. Once the background theory is completed, a discussion of sample fabrication is given followed by an explanation of the experimental procedure for measuring weak localization magnetoresistance. A brief explanation of the magnetoresistance results will also be discussed.

Chapter 3 begins with a discussion of some basic concepts of electrical noise such as thermal noise and the idea of noise power. The next topic is the theoretical background of universal conductance fluctuation theory. This includes a discussion of both the magnetic field-dependent universal conductance fluctuations as well as the time-dependent

universal conductance fluctuations and its magnetic field dependence. After the theoretical section, an explanation of the five-terminal noise measurement scheme will be given. Finally, some results of the noise measurement will be given.

Chapter 4 focuses on the results of the coherence length comparison in the three materials. First, the AuPd results will be given and implications of the results will be discussed. Then, the Ag results will be shown and discussed. A discussion of coherence saturation and its possible causes will also appear in this section of the chapter. Finally, the results of the Au experiments will be discussed. This discussion will conclude with mention of what the results may imply about the two level system distribution in normal metals.

The concluding chapter 5 will discuss possible directions of continued study while summarizing the results of this thesis. The chapter will close with some concluding remarks about the state of this area of condensed matter physics.

Chapter 2

Weak Localization

2.1 Theory

2.1.1 Quantum Diffusion

The quantum transport phenomenon known as weak localization builds on the concepts explaining the Aharonov-Bohm effect. Unlike the previous phenomenon, weak localization does not need a specific geometry to be observed. All that is needed for weak localization is a metal with looped electronic trajectories.

As in classical diffusion, an electron will propagate through a metal colliding (elastically) into defects that randomize its momentum and phase. However, unlike classical diffusion, the phase of the electron's wave function is important. In essence, the initial phase of the electron is "remembered" after each elastic scattering event. Thus the electron's partial wave functions retain the ability to interfere with one another. As previously mentioned, once the electron experiences enough of the three dephasing interactions, its coherence is lost and the electron can be treated classically. The idea of coherence and quantum interference is in stark contrast to the concept of a Markov process.

It has already been shown that the electron's probability to be at any point B after propagating from point A has an interference term. However, in a typical disordered metal there should be many paths that go from point A to B and each path should have some random phase shift. This would imply that the net interference occurring at point B should just average away to zero. This statement is only slightly incorrect, but

the small oversight explains the existence of weak localization. Given a time to diffuse through a metal, the electron has a Gaussian probability of being a distance r away from its initial point. This idea is graphed in Figure 2.2 [12]. This probability curve means that the electron has a high chance of returning to its starting point. Every returning path, however, should also be paired with a path that is merely time-reversed, but has an identical phase. The idea is shown below in Figure 2.1 [12].

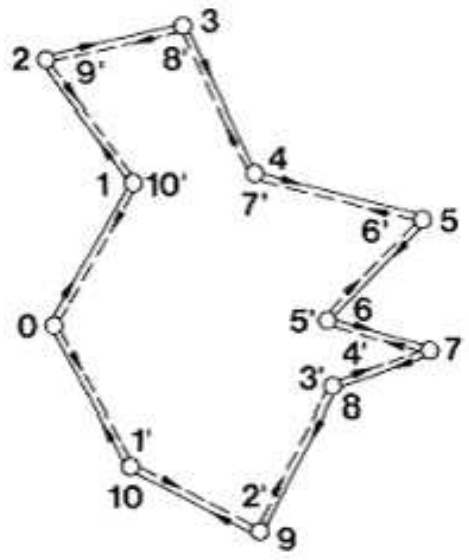

Figure 2.1: An electron starting at point 0 can return to 0 via the unprimed path or primed path. The primed path is simply the time reversal of the unprimed path.

A path and its time-reversed path should result in the electron having the same phase when it returns (as long as the scattering processes are elastic). Therefore, the two paths should constructively interfere according to equation 1.3.2. The fact the constructive interference occurs at the initial position of the path means there is an enhanced probability that the electron will have a net displacement of zero. Said another way, the interference term of the probability will cause a localization of the electron. Since the electron has

returned to its initial point via elastic scattering, its momentum is equal in magnitude (the assumption that the electron has returned to its initial position via elastic scattering is valid since $L_{\text{in}} \gg l_{\text{e}}$ in most disordered metals at the temperatures of interest). However, the net momentum direction compared with its initial momentum will be opposite. Because of this, weak localization can be thought of as enhanced backscattering. The fact that the electron has a higher probability of backscattering should decrease the conductivity of the metal.

To find the conductivity correction due to this localization, it is necessary to determine the probability for an electron to return to its starting position. With this, the conductivity correction can be found using the equation 2.1.1 [13]:

$$\Delta\sigma = -\frac{4e^2 D}{h}\int_0^\infty P(0,t)dt \tag{2.1.1}$$

$P(\vec{x},t)$ is the probability of the electron moving a displacement $\vec{x}$ in time t.

Since the electron's motion inside a metal is diffusive, its probability should obey the diffusion equation for motion away from point source:

$$\left(\frac{\partial}{\partial t} - D\nabla^2\right) P(\vec{x},t) = \delta(\vec{x})\delta(t) \tag{2.1.2}$$

The full solution to this equation is not easily determined, however, the general solution is just that of the standard diffusion equation. Fortunately, since the probability of interest is at a displacement of zero, the modal solution is not relevant to the following discussion. The solution to the general diffusion equation is:

$$P(\vec{x},t) = \frac{1}{(4\pi Dt)^{d/2}}\exp\left(-\frac{|\vec{x}|^2}{4Dt}\right) \tag{2.1.3}$$

Since the probability of interest has a displacement of zero, the exponential term of

equation 2.1.3 will be one. Two corrections to this probability also need to be made. One comes from the fact that there is a probability that the returning electron has lost its coherence. The other comes about since the electron has a probability not to scatter at all in time t. If the electron experiences no scattering it has no probability to change its momentum. It, therefore, has no means of returning to its initial position. The corrected probability takes the form:

$$P(0,t) = \frac{\exp(-t/\tau_\phi)}{(4\pi Dt)^{d/2}}[1 - \exp(-t/\tau)] \tag{2.1.4}$$

Plugging this into equation 2.1.1 gives a conductivity correction in each dimension of:

Table 2.1: The WL conductivity correction, $\Delta\sigma$, for each dimension.

d	$\Delta\sigma$
1	$-\frac{e^2}{\pi\hbar}L_\phi\left(1-\sqrt{\frac{\tau}{\tau+\tau_\phi}}\right)$
2	$-\frac{e^2}{2\pi^2\hbar}\ln\left(1+\frac{\tau_\phi}{\tau}\right)$
3	$-\frac{e^2}{2\pi^2\hbar L_\phi}\left(\sqrt{1+\frac{\tau_\phi}{\tau}}-1\right)$

Notice that the disorder of the sample (relaxation time) and dephasing mechanisms (coherence length) affects the conductivity in different ways for each dimension. In all

three cases, however, as the coherence length decreases, the conductivity correction becomes smaller, and as the relaxation time increases, the conductivity correction decreases. This means that a high degree of disorder will increase the conductivity correction due to weak localization. An interesting point to make about the previous derivation is that it derived using classical physics. All of the quantum mechanics is embedded in the coherence time. A rigorous quantum derivation of these corrections using a Green's function approach has been performed and yields identical results [13].

2.1.2 Spin-Orbit Interaction

Another topic within weak localization that needs exploring is the spin-orbit interaction effect. An electron propagating through a metal sees the ion cores as moving positive charges. Each moving charge creates a magnetic field that acts to rotate the electron's spin. To find the effect of the spin-orbit interaction, one must consider the spin component of the electron's wave function and how a rotated spin affects the interference due to enhanced backscattering. The argument starts by introducing a rotation matrix, R, which acts on the spin of the electron [10].

$$R = \begin{pmatrix} \cos\left(\frac{\alpha}{2}\right)\exp\left(i\frac{\beta+\gamma}{2}\right) & -i\sin\left(\frac{\alpha}{2}\right)\exp\left(-i\frac{\beta-\gamma}{2}\right) \\ i\sin\left(\frac{\alpha}{2}\right)\exp\left(i\frac{\beta-\gamma}{2}\right) & \cos\left(\frac{\alpha}{2}\right)\exp\left(-i\frac{\beta+\gamma}{2}\right) \end{pmatrix} \tag{2.1.5}$$

The values α, β, and γ represent the angle of rotation away from the z, x, and y-axis respectively.

After experiencing a spin-orbit scattering events while traveling down a specific path, the resultant electron spin should become:

$$|s'\rangle = R\,|s\rangle \tag{2.1.6}$$

If said path has a symmetrically time-reversed path, its resultant spin will be:

$$|s''\rangle = R^{-1}\,|s\rangle \tag{2.1.7}$$

Therefore, the interference term between the two paths should contain the value:

$$\langle s''|s'\rangle = \langle s|R^2|s\rangle \tag{2.1.8}$$

where

$$R^2 = \begin{pmatrix} \cos^2\left(\frac{\alpha}{2}\right)\exp\left[i(\beta+\gamma)\right] - \sin^2\left(\frac{\alpha}{2}\right) & \frac{i}{2}\sin(\alpha)[\exp(-i\beta)+\exp(i\gamma)] \\ \frac{i}{2}\sin(\alpha)[\exp(i\beta)+\exp(-i\gamma)] & \cos^2\left(\frac{\alpha}{2}\right)\exp\left[-i(\beta+\gamma)\right] - \sin^2\left(\frac{\alpha}{2}\right) \end{pmatrix} \tag{2.1.9}$$

Equation 2.1.8 selects out the diagonal elements of equation 2.1.9 and is determined by the spin direction. When there is no spin-orbit scattering, no rotation of the spin occurs meaning that all three angles of rotation are zero. All three angles set to zero give a value of 1 for 2.1.8, meaning no spin-orbit correction is necessary. In the limit of strong spin-orbit scattering, the rotation angles can take any value and therefore the average value of equation 2.1.8 must be calculated. The average for both $\sin^2(x)$ and $\cos^2(x)$ is 1/2 while the average for the complex exponential is zero (it is more clearly seen by using Euler's Identity to change the exponential to a complex function of a cosine and sine function). Using the results of the three average values leads to equation 2.1.8 equaling -1/2. This means that in the strong spin-orbit coupling limit, the probability of finding a particle at its initial point after time t is actually half of the classical probability. In other words, a weak antilocalization is produced. A plot representing the probability of the electron for each spin-orbit interaction case is given in Figure 2.2.

The spin-orbit interaction also introduces an intrinsic spin-flip scattering process that must be considered when finding the total coherence length of a system. To understand

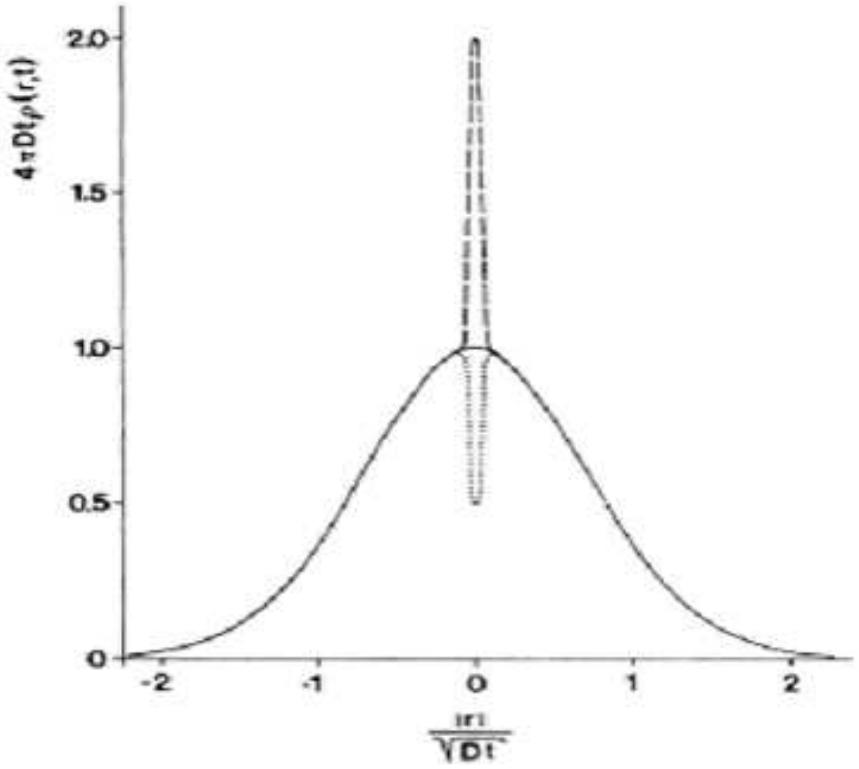

Figure 2.2: The solid line represents the classical probability. The long-dashed line represents the quantum-corrected probability, and the dotted line represents the quantum-corrected probability with strong spin-orbit coupling. This plot is an over-simplification since the integral under each curve must result in the same value!

this correction, one must consider the total angular momentum of the system. Consider the partial wave function of a loop trajectory and its time-reversed conjugate. Upon interference, the partial wave functions become entangled and the total angular momentum, J, becomes the important quantity. The possible spin states of the entangled wave function are:

$$\begin{array}{ll} |\uparrow\downarrow\rangle - |\downarrow\uparrow\rangle & J = 0 \\ |\uparrow\uparrow\rangle\,,\ |\downarrow\downarrow\rangle\,,\ |\uparrow\downarrow\rangle + |\downarrow\uparrow\rangle & J = 1 \end{array} \tag{2.1.10}$$

The result of the entanglement is a singlet state with $J = 0$ and a triplet channel with $J = 1$. Only a state with a non-zero J is influenced by the perceived magnetic field due

to the atomic nuclei. Therefore, an extra dephasing mechanism must be considered when finding the total coherence length of an electron, but must be weighted accordingly. The correction to the coherence time due to the triplet channel becomes [14]:

$$\frac{1}{\tau_\phi} = \frac{1}{\tau_{\rm in}} + \frac{4}{3\tau_{\rm so}} \tag{2.1.11}$$

2.1.3 Weak Localization Magnetoresistance

As was shown in the Aharonov-Bohm effect, the introduction of a perpendicular magnetic field causes a phase shift of the electron's partial wave function. This magnetic field-induced phase shift manifests itself in weak localization as a magnetoresistance. This magnetoresistance provides the necessary means of inferring phase coherence information, as will be seen shortly.

The method to find the theoretical magnetoresistance prediction is an extremely complicated problem more appropriately left for a theoretical physicist to explain [13]. The main points of the pertubative calculation are that the electrons are treated as non-interacting particles (the e-e interaction is treated in the coherence time,) and that the net disorder of the metal is weak ($(k_{\rm f}l)^{-1} \ll 1$). However, there is a semi-classical approach that combines the above calculation of the weak localization conductivity correction and the standard Landau level problem seen in undergraduate quantum mechanics courses (however it is a bit more difficult to solve completely) [13]. The results of this calculation are adequate for the purpose of giving a qualitative understanding of the importance of a magnetic field with regards to weak localization. The starting point is to rewrite equation 2.1.2 with the typical magnetic potential term (note that the diffusion equation is being used instead of the Schrodinger wave equation like in the typical Landau level

problem).

$$\left[\frac{\partial}{\partial t} - D\left(i\frac{\hat{\mathbf{p}}_x + \hat{\mathbf{p}}_y}{\hbar} - i\frac{2e\vec{A}}{\hbar}\right)^2 + \frac{1}{\tau_\phi}\right] P(\vec{x},t) = \delta(\vec{x})\delta(t) \tag{2.1.12}$$

Equation 2.1.12 is written assuming the system of interest is two-dimensional with the magnetic field oriented perpendicular to the plane of the system. Not surprising, it is convenient to use the Landau gauge to express the vector potential.

Two parts of equation 2.1.12 need explanation. The first is the $1/\tau_\phi$ term. This is simply the term that will introduce the correction to the probability dealing with the likelihood of the electron remaining phase coherent. The second is the factor of 2 in the momentum substitution due to the magnetic vector potential. Unfortunately, it cannot be explained in this semi-classical approach. As mentioned earlier, a full quantum treatment of weak localization can be worked out. Such a treatment involves using complicated Green's functions and ladder diagrams. However, the basic premise is a phase shift contribution arises from both a path and its time reversed conjugate so the total phase shift must have a factor of two. In "theory language" the explanation involves a phase shift coming from both the electron line and hole line of the diagram representing the relevant Green's function resulting in a doubly charged particle.

Next is to use the Landau gauge to rewrite equation 2.1.12 in terms of $\vec{B}$ instead of $\vec{A}$ as well as making the assumption that the separable solution along the y-axis is just that of a plane wave with wave number k. Therefore, equation 2.1.12 can be rewritten as:

$$\left[\frac{\partial}{\partial t} - D\frac{\partial^2}{\partial x^2} + D\left(k - \frac{2eBx}{\hbar}\right)^2 + \frac{1}{\tau_\phi}\right] P(\vec{x},t) = \delta(\vec{x})\delta(t) \tag{2.1.13}$$

The one fact to remember while going from equation 2.1.12 to equation 2.1.13 is the

commutation relation $[\hat{\mathbf{p}}_y, \hat{\mathbf{x}}] = 0$.

Fortunately, the solution of interest is at $x = 0$. The result of equation 2.1.13 is to just replace the coherence length with:

$$\frac{1}{\tau_\phi} \rightarrow \frac{1}{\tau_\phi} + \frac{4eBD}{\hbar}(n + 1/2) \tag{2.1.14}$$

In order to find the magnetic field-dependent conductivity change would not only require the time integration stipulated in equation 2.1.1, but would also require a summation over all the occupied Landau levels. Unfortunately, even if these calculations were made, the resulting functional dependence of the magnetoresistance would be slightly incorrect. What equation 2.1.14 shows, however, is that a perpendicular magnetic field acts as an important dephasing mechanism. The magnetic field term can be thought of as a probability that the vector potential has randomized the phase of a looped path such that it no longer contributes to the weak localization correction to the conductivity.

The size of the magnetic field term in equation 2.1.14 can actually be explained physically by returning to the ideas introduced by the Aharanov-Bohm effect discussion. Qualitatively, one would expect that once a looped path's phase has been shifted by order unity, the phase of the path and its time-reversed conjugate would be sufficiently randomized to cease contributing to the weak localization effect. In this case, full loops (opposed to the half loops in the Aharanov-Bohm effect) are being considered so the phase change from a perpendicular magnetic field should be:

$$\Delta\phi = \frac{2e}{\hbar}\Phi \tag{2.1.15}$$

This means when the flux is equal to $\hbar/2e$, the flux condition is met. Since the loops are traced via diffusive motion, Einstein's equation for the variance of the displacement

of a diffusing particle should suffice for the area of the loop [15] resulting in a threaded flux of:

$$\Phi \cong (2Dt)B \tag{2.1.16}$$

Using the previous two equations and solving for 1/t returns the magnetic field contribution to the weak localization seen in equation 2.1.14.

2.1.4 Electron-electron Interaction

The WL magnetoresistance is the most well-established means of inferring coherence length information in normal metals. It has been used in countless experiments since the early 1980s [16, 17, 18, 19]. This tool has even been used to try and explore phase coherence in ferromagnetic films [20]. Why, though, is this measurement used so frequently while the measurement of resistance versus temperature almost never used. The answer is quite subtle. Of course, above a certain temperature, the electron-phonon scattering results in a temperature-dependent conductivity. However, even below this critical temperature there still exists temperature-dependent conductivity corrections that have nothing to due with quantum interference.

When developing the conductivity corrections due to Weak Localization, the electron-electron interactions are considered only in the total coherence length of each electronic wave function. In other words, the weak localization theory is predicated on a non-interacting electron picture. Therefore, no possible conductivity correction due to electron-electron interactions has been explored. It has been shown that such a correction is indeed expected due to exchange interactions between electrons [21]. Again, the details of the calculation involve complicated diagrammatic methods beyond the scope of

this thesis. Physically, the results of the treatment show that at low temperatures, the Coulomb interaction creates a "migration" of electron states away from the Fermi energy. This lowered number of states coupled with the reduced thermal energy of the electrons results in fewer available states for conduction electrons to occupy. Experimentally, this is observed as an increased resistivity with decreasing temperature. This result is of the utmost importance as the resulting conductivity correction will have the same temperature dependence as the weak localization correction (assuming the dominant dephasing mechanism is electron-electron scattering and no spin-orbit interaction). Therefore, it becomes quite difficult to separate the two corrections when measuring resistance versus temperature. To better illustrate the idea, Figure 2.3 shows the resistivity of a AuPd wire at both 0 T and 4 T. At 4 T, the WL correction is completely eliminated. Fortunately, the electron-electron interaction conductivity correction has no low order dependence on an applied magnetic field. This fact allows the experimental observation of the weak localization magnetoresistance without complications arising due to other conductivity corrections.

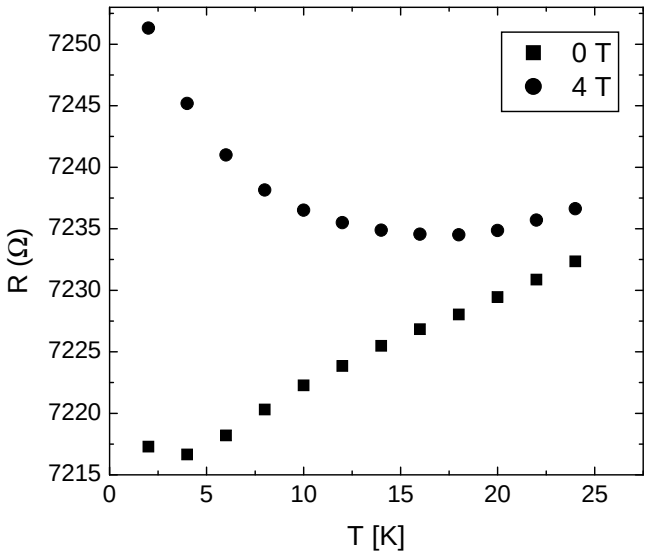

Figure 2.3: The temperature dependence of a 43 nm wide AuPd nanowire. The 4 T curve clearly shows that the WL correction to the resistivity is not the only low temperature correction that exists in this weakly disordered metal alloy.

2.2 Experimental Results

2.2.1 Sample Fabrication

Before discussing the experimental results of the weak localization measurements, it is necessary to discuss how the measured samples were fabricated. Sample preparation begins by cleaving 5 mm by 5 mm chips of undoped GaAs. The chips were then cleaned using lintless swabs soaked in acetone. After swabbing the surface, the chip was then placed under a UV lamp for 5 minutes to remove any remaining residue on the surface. Once a clean surface was achieved, resist was spun-cast onto the surface. 950 PMMA was used to create quasi-2D AuPd wires while 495 PMMA was used to create all the quasi-1D wires. After spin-casting, samples were then placed on a hot plate for an hour at 165 °C to evaporate away the solvent in the resist.

Once the chips finished baking, they were ready to be patterned. All samples were patterned using standard single-layer electron beam lithography. An example of the resultant pattern is given in Figure 2.4.

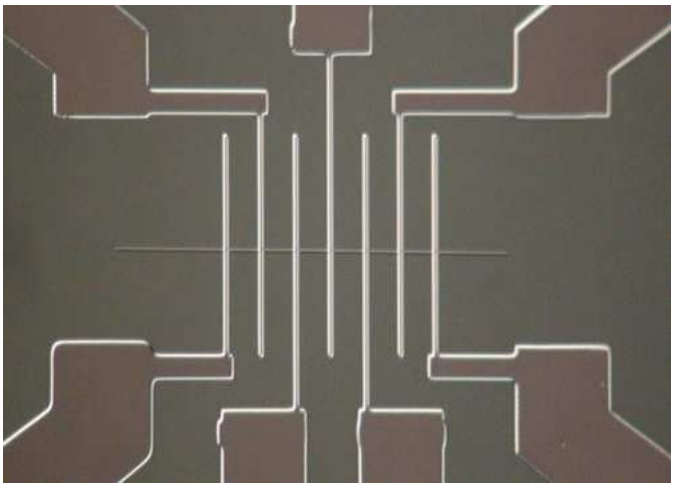

Figure 2.4: The lead-wire pattern used to fabricate all the measured samples. The leads start from large contact pads and taper down to the leads in the image.

The lithography procedure was concluded by evaporating the desired metal onto the chip using an electron beam evaporator. The in-lab Edwards Auto 306 evaporator was used to deposit AuPd and Ag while a Sharon rig located in the shared equipment clean room was used for the Au samples. The AuPd was 60 % Au and 40 %. The Ag was 99.99 % pure and the Au was 99.9999 % pure. Some of the Au samples used a 99.995 % pure Ti adhesion layer of 1.5 nm. Liftoff was accomplished using acetone for evaporations performed in the Edwards evaporator while chloroform was needed when using the Sharon system. The reason the chloroform was necessary is still unclear.

It should be noted that Ti/Au leads were used during the AuPd measurements. This was done strictly to keep consistent with previously performed QTP experiments with

AuPd [18]. Two lithography steps were necessary to produce such a structure. To limit contact resistances, oxygen plasma cleaning was used after the second lift-off procedure (used to define the leads).

2.2.2 Magnetoresistance Measurement Scheme

Once sample fabrication was finished, the sample was attached to a DC resistivity puck designed for insertion into a Quantum Design physical properties measurement system (PPMS). The PPMS is an open cycle ^{4}He cryostat with a 9 T superconducting magnet. Samples were "glued" to the puck with Apiezon N grease and wired using uninsulated 99.99 % Au wire and indium solder joints.

After wiring the sample to the resistivity puck, two-terminal resistance measurements were made on adjacent lead pairs to test for broken leads and/or wire segments. After a successful two-terminal test, the sample was cooled to 2 K. After cooling was finished, a four terminal resistance circuit was setup. The circuit schematic is shown in Figure 2.5. The resistor, R_b, is a ballast resistor used to turn the voltage source into a current source. The lock-in then measured the voltage difference between the two voltage leads. By using Ohm's law and the known current and measured voltage difference, the resistance of the measured sample segment could be found.

The ac voltage was supplied by a Stanford Research Systems model SR830 DSP lock-in amplifier. The voltage frequency was set between 700 Hz and 1 KHz depending on what material sample was being measured. The ballast resistor, R_b, was either 1, 10, or 100 MΩ depending on the desired current. The measured signal is demodulated using the same SR830 lock-in that is acting as the voltage source.

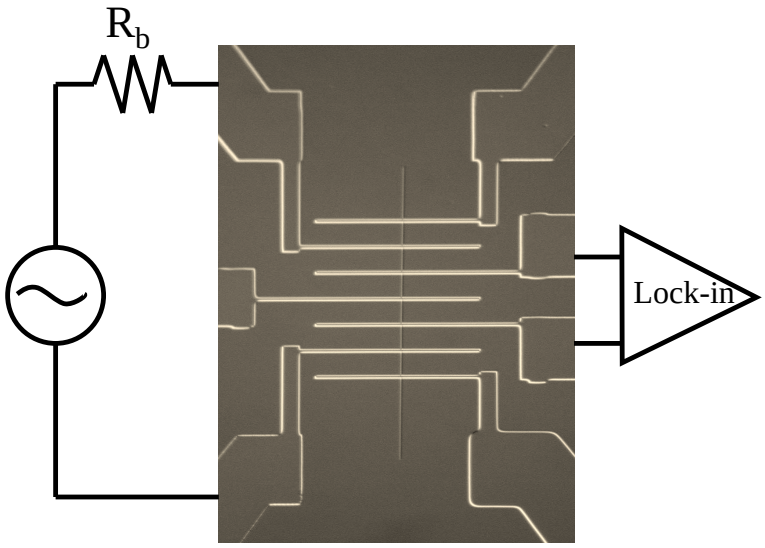

Figure 2.5: The ac four terminal resistance measurement schematic.

The magnetoresistance measurement is made by sitting at discrete, evenly-spaced magnetic field strengths for roughly a minute at each point. The resistance is measured every second and then all the data points at each field are averaged to determine the resistance value at each field strength. All data sorting was performed in Microsoft Excel. Typically, 61 field strengths were measured with an equal number for each polarity of the magnetic field. The magnetoresistance was measured at 2, 4, 6, 8, 10, and 14 K in all materials and was measured at 20 K as well in AuPd. Examples of the resultant magnetoresistances for each material are given in Figures 2.6, 2.7, and 2.8. The curves show only field points above 0. However, these points actually represent the average of both field polarities.

There are a few points worth noting about these magnetoresistance plots. One is the sign of the magnetoresistance. Both the AuPd and Au show an increased resistance

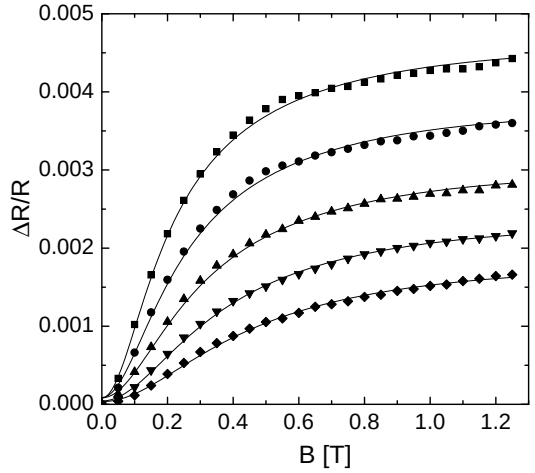

Figure 2.6: The magnetoresistance of a 43 nm wide AuPd wire. The data is at 2 (■), 4 (●), 6 (▲), 8 (▼), and 10 (◆) K. $\Delta R/R$ is defined as $\frac{\mathrm{R(B)-R(B=\infty)}}{\mathrm{R(B=\infty)}}$. The data has been offset for clarity.

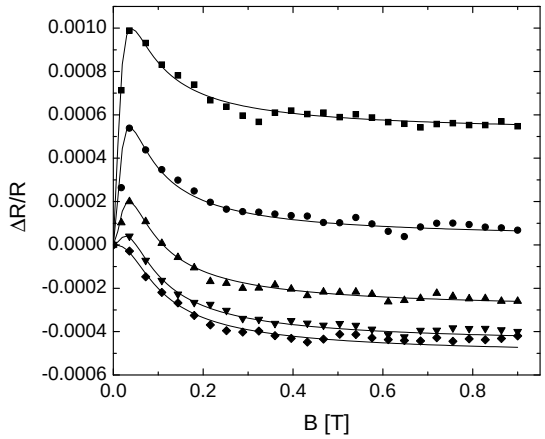

Figure 2.7: The magnetoresistance of a 140 nm wide Ag wire. The data is at 2 (■), 4 (●), 6 (▲), 8 (▼), and 10 (◆) K. $\Delta R/R$ is defined as $\frac{\mathrm{R(B)-R(B=\infty)}}{\mathrm{R(B=\infty)}}$. The data has been offset for clarity.

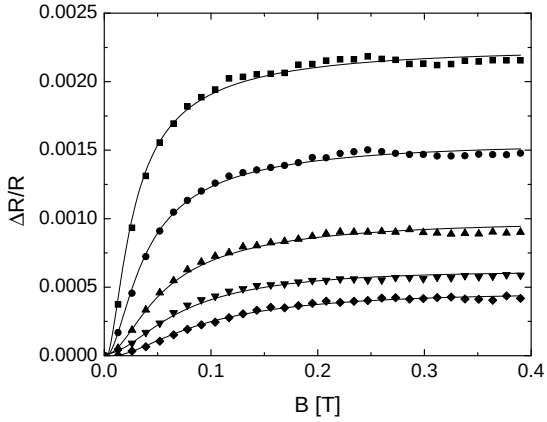

Figure 2.8: The magnetoresistance of a 70 nm wide Au wire without a Ti adhesion layer. The data is at 2 (■), 4 (●), 6 (▲), 8 (▼), and 10 (◆) K. $\Delta R/R$ is defined as $\frac{\mathrm{R(B)-R(B=\infty)}}{\mathrm{R(B=\infty)}}$. The data has been offset for clarity.

as the applied field suppresses partial wave function interference. This means these two materials exhibit a weak antilocalization and are thus in the strong spin-orbit regime. The Ag has a more complicated curve. At low fields the resistance gets larger, consistent with weak antilocalization. However, at larger fields, the resistance starts to drop, consistent with weak localization. The explanation for this is that Ag is in the intermediate spin-orbit regime ($L_\phi \approx L_{\mathrm{so}}$). At low fields, the only phases the field will randomize are those associated with the paths with the longest circumference. Those paths, however, will have the greatest probability of undergoing a spin-orbit scattering event. This means that these paths should create an antilocalization effect. As the shorter circumference paths' phases are randomized, interference effects from paths that have not undergone a spin-orbit scattering event will be suppressed. In other words, paths contributing to a weak localization will be eliminated resulting in a reduced resistance. By defining a magnetic length, $L_{\mathrm{B}} \equiv \sqrt{\frac{\hbar}{2eB}}$, it can easily be shown when this crossover from weak antilocalization to weak localization occurs. L_{B} is simply the length over which a square of side L_{B} will have one flux quantum threaded through it. When $L_{\mathrm{B}} \approx L_{\mathrm{so}}$, the antilocalization-localization crossover should occur.

A second point is the field scale over which the magnetoresistance change occurs. Qualitatively, the field scale goes inversely with the width of the wire. This should not be surprising. As the sample width is reduced for a fixed L_ϕ, the coherent loops become narrower. Such loops sweep out a much smaller area. This means that a larger magnetic field is required to pass the necessary flux through the path to randomize its phase.

Later, a rigorous discussion of how the coherence lengths were inferred from the WL magnetoresistance will be given. For now, though, the theory and experimental results

lay a firm foundation for understanding the work done in this thesis. A similar foundation must be laid for the other theory discussed in these pages, universal conductance fluctuation theory.

Chapter 3

Universal Conductance Fluctuation Theory

3.1 Theory

3.1.1 Thermal Noise

Before exploring universal conductance fluctuation theory, a brief review of the different forms of noise is necessary. In the systems of interest, two noise sources are important. The first is Johnson or thermal noise. The second is excess or $1/f$ noise. A brief derivation of thermal noise will be given below.

Thermal noise can be attributed to the thermally agitated Brownian motion of the electrons in a metal. The noise was first observed in 1928 by John B. Johnson [22] hence the name Johnson noise. H. Nyquist performed the theoretical derivation of Johnson noise at the same time [23] (the two papers are actually back-to-back in Physical Review) using nothing more than classical statistics, thermodynamics, and basic electronics. The derivation starts by imagining a circuit with two identical resistors connected with non-dissipative wires of length L. A picture of the circuit is given in Figure 3.1 [23]. Using periodic boundary conditions $V(0) = V(L)$, and noting that the system can be treated as vibrating standing waves, a density of modes can be calculated. The derivation begins by writing down the frequencies of the standing waves, $f = \frac{nc}{2L}$. The density of modes in a given bandwidth, Δf, should be:

$$D(f)\Delta f = \frac{\partial n}{\partial f}\Delta f = \frac{2L}{c}\Delta f \tag{3.1.1}$$

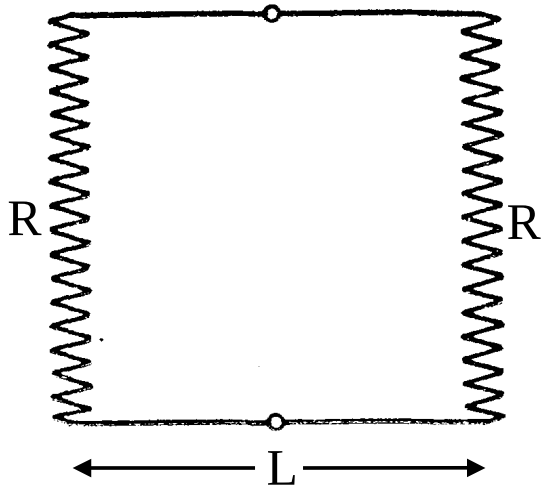

Figure 3.1: The circuit used by Nyquist to derive the expression for thermal noise power.

Using the Boltzmann distribution, the mean energy per mode is $k_{\mathrm{B}}T$. Multiplying this energy per mode with the density of modes gives an energy density of $\frac{2Lk_{\mathrm{B}}T}{c}\Delta f$. The time of flight for a wave to travel between resistors is $\Delta t = \frac{L}{c}$. Only half the total energy should be traveling in the direction of interest, however. Therefore, the total power can be written as:

$$P(f)\Delta f = k_{\mathrm{B}}T\Delta f \tag{3.1.2}$$

There is a second way to calculate the power in the circuit. The power dissipated by a resistor is I^2R. For this circuit, the dissipated energy from one of the resistors should be:

$$P(f)\Delta f = I^2R\Delta f = \frac{V^2}{4R^2}R\Delta f = \frac{V^2}{4R}\Delta f \tag{3.1.3}$$

Combining equations 3.1.2 and 3.1.3 results in:

$$V^2\Delta f = 4k_{\mathrm{B}}TR\Delta f \tag{3.1.4}$$

Equation 3.1.4 has no frequency dependence so the time average of V^2 should be:

$$\left\langle V^2 \right\rangle_{\text{time}} = 4k_{\text{B}}TR\Delta f \tag{3.1.5}$$

The important results of equation 3.1.5 are the thermal noise has no frequency dependence and it has a linear temperature dependence. Noise without a frequency dependence is referred to as white noise. The linear temperature dependence means that the thermal noise at the temperatures of the interest in this thesis should be quite small. However, Johnson noise plays an important role nonetheless. Remember, the same Brownian motion that causes thermal noise is also causing electron dephasing. The previous derivation helps form the physical basis for calculating equations 1.3.4 and 1.3.5.

One other idea needs mentioning before continuing. The question of how noise sources add can be easily explained using the previous derivation. If the two resistors are each replaced by two resistors in series, then the result of the Johnson noise derivation should become:

$$\left\langle V^2 \right\rangle_{\text{time}} = 8k_{\text{B}}TR\Delta f = 4k_{\text{B}}TR\Delta f + 4k_{\text{B}}TR\Delta f \tag{3.1.6}$$

Hence, noise should add in quadrature. Typically noise is reported in units of $\text{V}/\sqrt{\text{Hz}}$. However, it is the square of this value that adds. Due to this fact, noise measurements will always be reported in units related to V^2/Hz, known as the noise power, in this thesis.

3.1.2 The Local Interference Model

Unlike Johnson noise, the excess noise seen in the systems of interest is not caused by random electron motion. It is a result of impurity motion. The excess noise has two very important characteristics that need discussion. One is the $1/f$ dependence (pink noise)

and the other is its temperature dependence. Both of these characteristics are explained with classical statistics until temperatures below ∼30 K. Once this temperature range is reached, the classical model fails to explain an upturn in the $1/f$ noise power as temperature is decreased.

The model starts by considering an impurity with two distinct scattering cross sections. This can be accomplished if the defect is moving between two locations. The idea of a defect with two discernable cross sections will be referred to as a two level system (TLS) repeatedly in this thesis. Each scattering cross section will result in a slightly different contribution to the net conductivity of the system. For a system with just a single TLS, a measure of conductivity versus time would result in observable jumps between the two conductivities. Such a signal is referred to as telegraph noise. Since a TLS switches states at random, it should display a Debye-Lorentzian noise power [24]. This has the form:

$$S(\omega) \propto \frac{\tau}{(\omega\tau)^2 + 1} \tag{3.1.7}$$

where τ is the characteristic time of the TLS. In the case of a TLS, the characteristic time should just be:

$$\tau^{-1} = \tau_1^{-1} + \tau_2^{-1} \tag{3.1.8}$$

where τ_1 and τ_2 are just the average time spent in each state.

In the systems of interest, there should exist a large number of TLS with a broad range of characteristics times. To determine the resultant noise power can be accomplished by integrating the Debye-Lorentzian spectrum over τ.

$$S(\omega) \propto \int \frac{D(\tau)\tau}{(\omega\tau)^2 + 1} d\tau \tag{3.1.9}$$

$D(\tau)$ is the distribution function of the characteristic times. If $D(\tau)$ is proportional to $1/\tau$, then the power spectrum will have an inverse frequency dependence.

In the high temperature limit, the available thermal energy is high enough to cause hopping of defects. The expected characteristic time scale for such a thermal fluctuator is [25]:

$$\tau = \tau_0 \exp\left(\frac{\Delta E}{k_{\mathrm{B}} T}\right) \tag{3.1.10}$$

where ΔE is the activation energy necessary to induce a defect to hop. Assuming that the distribution of necessary activation energies is flat, then it can be shown using the relation $D(V)dV = D(\tau)d\tau$ that $D(\tau)$ has a $1/\tau$ dependence.

In the low temperature limit, there is not enough thermal energy to expect many fluctuating defects. However, quantum tunneling must be considered as a mechanism by which a defect changes state. In this case, the tunneling time is related to both the barrier height V and the width d [26].

$$\tau = \tau_0 \exp\left[\left(\frac{2md^2V}{h^2}\right)^{1/2}\right] \tag{3.1.11}$$

Assuming that the distribution of tunneling barriers is flat for different values of V, then it can be shown that $D(\tau)$ has a $1/\tau$ dependence using the same argument as above.

The following shows that at both low and high temperatures, an excess noise with a $1/f$ spectrum should exist. However, the theory as it stands is not influenced by interference of electron paths. In fact, this theory treats each scattering event independently, another example of a Markovian process. This "classical" excess noise explanation is called the local interference model (as will shortly be seen, this is an unfortunate choice for the name of this effect). The name comes from the fact that every moving impurity

does not cause changes in the conductance of a sample. Imagine a large single crystal with a vacancy far from any surface. If the location of the vacancy moves one lattice site, its scattering cross section should not change. However, if the same vacancy is located near a surface (grain boundary), then the act of moving will change the scattering cross section of the vacancy due to the interplay between the location of the vacancy and surface. This interplay was coined "local interference."

Also of great importance is the amplitude of this excess noise. Clearly, the noise should depend on the number of mobile defects in the system of interest. The number of moving defects should depend on the available thermal energy. Therefore, the amplitude of the excess noise is expected to decrease as the temperature of the system is lowered. This is exactly what is observed experimentally at high temperatures. However, at low temperatures (below about 30 K), this excess noise is observed to increase [27]. The theory as it stands is not capable of explaining such an observance. The fact that the noise increases as the temperature is lowered makes quantum interference a prime candidate to explain the phenomenon.

3.1.3 The Magnetofingerprint

It has already been shown that the interference between partial wave functions of a conduction electron will affect the conductivity of a disordered metal. However, the previous phenomena, the Aharonov-Bohm effect and weak localization, are dependent on specific types of paths and are not directly dependent on the orientation of scattering sites. The paths that an electron may take while propagating through a disordered metal are completely dependent on the location of each scattering site and, thus, the interference

pattern produced by intersecting paths should also be specific to the location of each defect. The situation is analogous to performing a typical interference experiment with a coherent light source and a grating with many randomly placed slits. The resultant interference pattern will appear quite random, but will still represent the arrangement of the slits. By altering the slit (scattering site) arrangement, the interference pattern will also change. This is the essence of the QTP magnetic field-dependent universal conductance fluctuations, commonly called the magnetofingerprint.

The physical explanation of the magnetofingerprint is rooted in what was termed the ergodic hypothesis. This hypothesis states that any effect resulting in a change to the interference pattern of an electron's partial wave functions is equivalent to a change in the impurity configuration of the system [28]. Experimentally, such a fact is very important since changing the locations of sample impurities is extremely difficult. As was seen in the Aharonov-Bohm effect and weak localization, a perpendicular magnetic field will produce a phase change in each electron path. The actual phase shift of each partial wave function will be dependent on the strength of the magnetic field such that as the field is altered, so too will the resultant interference pattern. This also means that every field strength corresponds to a specific interference pattern that is reproducible each time that field is applied to the system. However, each system will have a unique arrangement of scattering sites so the resultant interference pattern is sample-specific. It has already been seen that such interference affects an electron's probability to diffuse through a metal, and that a metal's conductivity is directly related to this probability. Therefore a reproducible, sample-specific conductivity fluctuation should be observed in a diffusive metallic system as an applied perpendicular magnetic field is swept. This magnetoresistance is known as

the magnetofingerprint. An example of a magnetofingerprint at different temperatures is given in Figure 3.2.

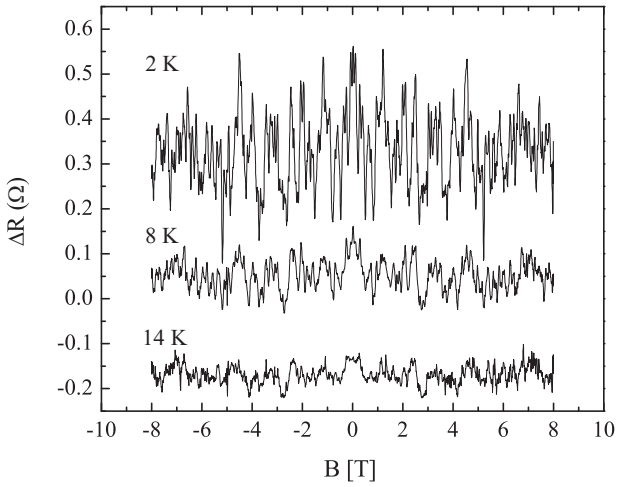

Figure 3.2: The magnetofingerprint of a 125 nm wide Ag wire. The features of the magnetofingerprint are reduced at higher temperatures due to the temperature dependence of the coherence length. Notice the symmetry of the magnetoresistance with respect to the magnetic field. The curves have been offset for clarity.

The size of these conductance fluctuations is a little more difficult to explain. An approximate size can be found using the Landauer formula. In the case of a disordered metal, each possible pair of starting and ending points an electron can pass through can be thought of as a conductance channel. The Landauer formula states:

$$G = \frac{e^2}{h} \sum_{i,j=1}^{N} |t_{ij}|^2 \tag{3.1.12}$$

The value t_{ij} is the transmission probability of the channel between starting point i and ending point j. N is the total number of channels. As the magnetic field is swept, specific channels will be turned on or off due to interference effects. So a rough estimate of the

conductance variance gives:

$$\Delta G^2 = \left\langle (G - \langle G \rangle)^2 \right\rangle \approx \left\langle \left(\pm \frac{e^2}{h} \right)^2 \right\rangle = \frac{e^4}{h^2} \tag{3.1.13}$$

Of course the transmission probability is not the same for each channel and is not going to be 1 so this is very much an oversimplification. However, the more rigorous derivation gives almost identical results.

One must ask, "Why then does the magnetofingerprint get smaller as the temperature increases?" The answer: the argument above does not account for the finite L_ϕ at $T \neq 0$. When the system size becomes longer than L_ϕ, averaging effects must be taken into account. These averaging effects will be discussed in detail in the next subsection.

3.1.4 Averaging Effects

In most measured systems, the length of the sample is much longer than the coherence length of the material. This means the measured magnetofingerprint will have a variance smaller than the universal limit. To calculate the expected size of the magnetofingerprint, simply treat each coherent volume as an independent fluctuator. From basic statistical analysis, it can be shown:

$$\left(\frac{\delta G}{G} \right)^2 = \frac{1}{N} \left(\frac{\delta G_\phi}{G_\phi} \right)^2 \tag{3.1.14}$$

This is really a calculation of the standard deviation of the mean conductance. G_ϕ is the conductance of one coherent volume and N is the number of coherent volumes in the sample. Clearly, both N and G_ϕ should be dependent on L_ϕ. This self-averaging alone can explain why the magnetofingerprint variance has a temperature dependence (since L_ϕ is temperature dependent). However, there are other averaging effects that must also

be considered if the actual temperature dependence of the magnetofingerprint variance is to be found.

The other effects arise due to the available energy states conduction electrons are able to occupy. Sometimes called the coherence energy, when $L_z \gg L_\phi$ the Thouless energy is defined as [29]:

$$E_c \equiv \frac{\hbar D}{L_\phi^2} \tag{3.1.15}$$

The Thouless energy defines a "width" to the energy levels in the conduction band. When $k_B T > E_c$, the electrons can access more than one Thouless width worth of available states. The transmission properties of each Thouless width are uncorrelated with the others, resulting in a thermal averaging that is dependent on the number of Thouless widths.

The standard way to treat this thermal averaging is to define a thermal length and compare it to the coherence length. The thermal length is defined as:

$$L_{th} \equiv \sqrt{\frac{\hbar D}{k_B T}} \tag{3.1.16}$$

$L_{th} < L_\phi$ is equivalent to $k_B T > E_c$. The thermal length will be an important length scale to keep in mind for the forthcoming discussions.

A second averaging effect associated with the Thouless energy is also possible. When $eV_\phi > E_c$, the same band splitting effect occurs. V_ϕ is the voltage drop across one coherent volume.

3.1.5 Time-dependent Universal Conductance Fluctuations

The discussion of the MFUCF introduces the idea that quantum interference from all paths can affect the conductivity of a metal. In the magnetofingerprint, the conductance

fluctuations are a result of "simulated" mobile TLS. Even at temperatures much lower than 300 K, there should be actual mobile TLS in a metal. These TLS should affect the conductance in a similar manner to the "simulated" mobile TLS. However, these fluctuations should be observed as a function of time, not magnetic field.

Since the two effects are so closely related, it would seem the magnetofingerprint variance derivation is a good place to start when attempting to calculate the size of the time-dependent conductance fluctuations. In this case, however, the conductance change can be written for a single mobile TLS as [30]:

$$\delta G_1^2 = \left\langle \left(G\{r_1, r_2, ..., r_N\} - G\{r_1 + \delta r, r_2, ..., r_N\} \right)^2 \right\rangle \tag{3.1.17}$$

where r_N is the location of the N'th impurity. Using diagrammatic methods [30], the resulting conductance change will be:

$$\delta G_1^2 \approx \left(\frac{e^2}{h}\right)^2 \left(\frac{\Omega}{N l_{\mathrm{e}}^d}\right) \left(\frac{L}{l_{\mathrm{e}}}\right)^{2-d} \alpha(k_f \delta r) \tag{3.1.18}$$

where $\alpha(k_f \delta r) = 1 - \left(\frac{\sin(x/2)}{x/2}\right)^2$ and Ω is the sample volume.

At finite temperature and in one dimension, $\left(\frac{L}{l_{\mathrm{e}}}\right)^{2-d}$ can be replaced with $\frac{L_\phi l_{\mathrm{e}}}{L_{\mathrm{x}} L_{\mathrm{y}}}$. L_{x} and L_{y} are the sample dimensions transverse to the current flow. There is a second substitution explained in an erratum to ref [30] [31]. $\frac{\Omega}{N l_{\mathrm{e}}^d}$ can be replaced with $(k_{\mathrm{f}} l_{\mathrm{e}})^{-2}$. So, the conductance change due to a single TLS in a 1D system will be:

$$\delta G_1^2 \approx \left(\frac{e^2}{h}\right)^2 (k_{\mathrm{f}} l_{\mathrm{e}})^{-2} \left(\frac{L_\phi l_{\mathrm{e}}}{L_{\mathrm{x}} L_{\mathrm{y}}}\right) \alpha(k_f \delta r) \tag{3.1.19}$$

Of course, there will be more impurities in a typical system. The net effect of multiple TLS is additive. This means that the total conductance variance within a coherent volume

should be:

$$\delta G_\phi^2 = \delta G_1^2 n_\mathrm{s}(T)\Omega_\phi \quad \Omega_\phi = \begin{cases} L_\mathrm{x}L_\mathrm{y}L_\phi & 1D \\ L_\mathrm{x}L_\phi^2 & 2D \\ L_\phi^3 & 3D \end{cases} \tag{3.1.20}$$

where $n_\mathrm{s}(T)$ is the concentration of TLS with changing scattering cross sections. It is important to note that equation 3.1.20 is bounded by the universal upper limit of e^2/h. The majority of the samples measured in this thesis fall in the 1D limit so the derivation will continue only for 1D.

Just as for the magnetofingerprint, the thermal averaging must be taken into account. When $L_\phi > L_\mathrm{th}$, equation 3.1.20 must be multiplied by $(L_\mathrm{th}/L_\phi)^2$. Since a typical sample is many coherent volumes long, the self-averaging must also be included. Equation 3.1.14 can be used. In the 1D case, $N = L_\phi/L_\mathrm{z}$ and $G = G_\phi/N$. Making all the necessary substitutions, the expected conductance change due to quantum interference is:

$$\delta G^2 \approx \left(\frac{e^2}{h}\right)^2 n_\mathrm{s}(T)\left(k_\mathrm{f} l_\mathrm{e}\right)^{-2}\left(\frac{l_\mathrm{e}L_\mathrm{th}^2 L_\phi^3}{L_\mathrm{z}^3}\right)\alpha(k_f\delta r) \tag{3.1.21}$$

To calculate the noise power from this change, the conductance change needs to be multiplied by equation 3.1.9. As will be explained in the next section of this chapter, the noise measured in the experiments for this thesis was voltage noise, not conductance noise. The voltage noise can be related to the conductance noise using the relation:

$$\left(\frac{\delta G}{G}\right)^2 = \left(\frac{\delta R}{R}\right)^2 = \left(\frac{\delta V}{V}\right)^2 = \left(\frac{\delta I}{I}\right)^2 \tag{3.1.22}$$

Using Ohm's law and the relation $G = 1/R$, the expected noise power should be:

$$S_\mathrm{V} \approx I^2 R^4 \delta G^2 \int \frac{D(\tau)\tau}{(\omega\tau)^2 + 1} d\tau \tag{3.1.23}$$

Simplifying equation 3.1.23 gives quite a bit of information about the temperature dependence of the noise power. The expected temperature dependence of $n_{\mathrm{s}}(T)$ is T while L_{th}^2 is proportional to T^{-1}. Those two terms cancel so the only temperature dependence is due to L_ϕ and R.

3.1.6 Magnetic Field-dependence of Time-dependent Universal Conductance Fluctuations

Much like WL, TDUCF have a magnetic field dependence. Unfortunately, the detailed derivation of this dependence is even more complicated than that of the WL magnetoresistance. Because of this, only the main points of the TDUCF field dependence derivation will be discussed.

To begin, the definitions of the cooperon and diffuson need to be given. The cooperon is a two-particle propagator often referred to as the set of particle-particle diagrams. The important characteristic of the cooperon is it's sensitivity to a perpendicular magnetic field. The diffuson is also a two-particle propagator reffered to as the set of particle-hole diagrams. The diffuson, unlike the cooperon, is insensitive to a perpendicular magnetic field. A visual explanation is shown in Figure 3.3 [32]. The cooperon, therefore, is pertinent to WL while the diffuson has no net contribution to that phenomenon. In TDUCF, however, both the cooperon and diffuson have an equal contribution to the net amplitude of the effect [32]. From this fact, the TDUCF amplitude should decrease by a factor of 2 in a magnetic field as the field induced phase shift eliminates the cooperon channel. The field scale over which this occurs should be dependent on the coherence length of the system.

The derivation in [32] begins by defining the crossover function, the functional form

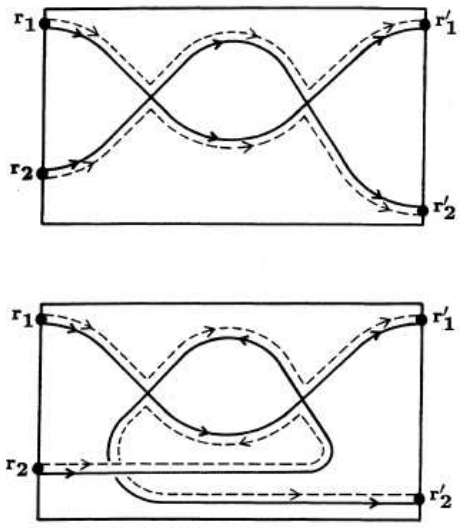

Figure 3.3: The top box shows four two-particle paths that would be part of the diffuson channel. The solid and dashed lines indicate the four paths. The addition of a perpendicular magnetic field would introduce identical phase shifts to the paths. The bottom box shows four two-particle paths that would be part of the cooperon channel. Since the dashed and solid lines traverse the looped part of the path in opposite directions, a perpendicular magnetic field will induce a phase difference between the solid and dashed paths.

of the TDUCF noise power with respect to magnetic field. It is defined as:

$$\nu(B) = \frac{N(B)}{N(B=0)} \tag{3.1.24}$$

where $N(B)$ is the integrated noise power. This ratio, though, should be equal to the ratio of the average conductance change as a function of magnetic field. It should also be reflective of only the cooperon channel. Using some tricky math, the conductance change can be found to be [32]:

$$\delta G^2 = \left\langle (G\{r_1, ..., r_N\} - G\{r_1 + \delta r, ..., r_N\})^2 \right\rangle \tag{3.1.25}$$

$$= \left\langle (G\{r_1, ..., r_N\} - \langle G\rangle - G\{r_1 + \delta r, ..., r_N\} + \langle G\rangle)^2 \right\rangle \tag{3.1.26}$$

$$\delta G^2 = 2[\Delta G^2 - \langle \Delta G\{r_1, ..., r_N\} \Delta G\{r_1 + \delta r, ..., r_N\}\rangle] \tag{3.1.27}$$

This holds as long as the two conductance values are assumed to have the same variance. Physically, equation 3.1.27 can be broken up into two parts. One is the magnetofingerprint conductance variance. The other is a reduction factor due to the "effectiveness" of the TLS to completely rearrange the interference pattern of the partial wave functions. Thus, the more correlated the conductance variances are at the two impurity positions, the smaller the size of the TDUCF.

It was shown by Altshuler and Spivak that $\Delta G\{r_1, ..., r_N\}\Delta G\{r_1 + \delta r, ..., r_N\}$ is calculated by replacing the coherence length [33]:

$$\tau_\phi'^{-1} \rightarrow \tau_\phi^{-1} + \tau^{-1}\left(1 + \frac{\langle VV' \rangle}{\langle V \rangle^2}\right) \tag{3.1.28}$$

where V and V' represent the two potentials created by the TLS arangements and τ is the elastic relaxation time. Stone showed that in the case of small variations in the potential, δG^2 will be:

$$\delta G^2 \approx -2\tau_\phi'^{-1}\frac{d\Delta G^2}{d\tau_\phi^{-1}} \tag{3.1.29}$$

which just arises from the definition of the derivative.

In the case of large variations in the potential, the change will be:

$$\delta G^2 \approx 2\Delta G^2 \tag{3.1.30}$$

since the second term in equation 3.1.27 will be zero. Thus, the crossover function will have **distinct forms**, depending on how effective the TLS are at changing their scattering cross sections. When the impurity potential change is large, the TDUCF will approach the universal limit and are considered **saturated**. When the impurity potential change is small, the noise power is considered **unsaturated**. It cannot be overemphasized how

important this last result is to analyzing the work of this thesis. For emphasis: the saturated and unsaturated crossover functions will have different functional forms, and the two forms are only valid for the limiting cases of small and large impurity potential changes!

The discussion of the crossover function to this point has shown that there are different forms depending on the size of the TDUCF noise power. Where, though, is the magnetic field dependence in equations 3.1.29 and 3.1.30? The variance ΔG^2 (again, the size of the magnetofingerprint [34]) is related to the energy-correlation function. The variance has the form:

$$\Delta G^2(B,T) \propto \int K(\Delta E/2k_{\mathrm{B}}T)F(\Delta E,B)d\Delta E \tag{3.1.31}$$

where $K(x) = (x\coth(x) - 1)\sinh^2(x)$ and $F(\Delta E, B)$ is the $T = 0$ energy-correlation function. The samples of interest in this thesis are metallic, so $F(\Delta E, B) = F(\Delta E = 0, B)$. Also, $F(\Delta E, B)$ can be broken into two equal parts, $F(\Delta E, B) = F_{\mathrm{C}}(\Delta E, B) + F_{\mathrm{D}}(\Delta E)$, the cooperon contribution and diffuson contribution. The two parts will be identical at $B = 0$, but only F_{C} will have a field dependence.

Physically, the zero temperature energy-correlation function in a metallic system should just be the auto-correlation function of the magnetofingerprint at a fixed temperature with the substitution $\Delta B \rightarrow 2B$. So, the magnetic field-dependence of the TDUCF should resemble the decay of the auto-correlation function of the MFUCF at corresponding temperatures. The factor of 2 reduction in the noise power mentioned earlier comes from the magnetic field dependence of the cooperon contribution to the correlation function.

3.1.7 Saturated/Unsaturated TDUCF Determination

Determining the regime of the TDUCF are in becomes paramount when trying to infer coherence length data from the magnetic field-dependence of the TDUCF. Since saturated TDUCF have a different magnetic field dependence than unsaturated TDUCF, using the incorrect crossover function can result in inferring an incorrect coherence length. There is an accepted experimental test to determine the regime of the observed TDUCF [27]. As was seen in the derivation of the crossover function, when TDUCF are saturated, the fluctuation size should be the same size as the magnetofingerprint variance. By comparing the integrated noise power with the variance of the MFUCF, it should be possible to determine whether the TDUCF are saturated or not. This is done by asking, "How many decades must the $1/f$ noise be integrated over in order to recover the MFUCF variance?" The physically reasonable limits on the characteristic times of TLS limit the integration to $\sim$20 decades [25]. So, if the required number of decades is much greater than 20, the noise is assumed to be in the unsaturated regime. Written mathematically, if $S_{\mathrm{G}} = \delta G^2/f$ then:

$$\frac{f_{\max}}{f_{\min}} = \exp\left(\frac{\Delta G^2}{\delta G^2}\right) \approx 20 \tag{3.1.32}$$

if the TDUCF are saturated.

3.2 Experimental Results

3.2.1 Noise Measurement Scheme

The samples used to measure the WL magnetoresistance were also used to measure both the magnetofingerprint and the TDUCF. No, further discussion of sample fabrication is necessary for the discussion of measuring UCF of any kind.

The discussion of how the UCF measurements were made requires quite a bit more examination of the typical resistance measurements. Especially in the case of the TDUCF, the effect is small and other noise sources within the measurement circuit can become restrictively large.

In a typical dc four-terminal resistance measurement, there will be two very important noise sources to consider. One is the noise in the current source. In a circuit setup with a current source like that in 2.5, the drive noise will be due primarily due to the $1/f$ noise in the ballast resistor. The other major source of noise is in the amplification of the measured signal. This noise is pink as well. Any attempt to measure $1/f$ noise with a dc drive would be very difficult unless the size of the sample noise is much larger than the sum of the other two noise powers. By using an ac drive, the pink noise of the amplifier will become a white noise (the size of which is just the size of the pink noise at the drive frequency). By examining the noise contours of the amplifier, a frequency that minimizes the amplifier noise can be used. However, the ac four-terminal measurement is still sensitive to fluctuations in the drive current.

The standard method to eliminate sensitivity to the drive current in resistance measurements is to use a resistance bridge circuit. The most well known is Wheatstone bridge. A slightly modified version of this bridge setup is what was used to make all the noise measurements reported in this thesis.

A standard wheatstone bridge is shown in Figure 3.4. In the case of Figure 3.4, the bridge is being used to measure the resistance of resistor R_x. This is done by trying to null the voltage difference between the two sides of the bridge. This "balance point" is achieved when $R_x/R_1 = R_3/R_2$. Note that the result has no dependence on the drive

voltage or current. Thus, the measurement of R_x should be insensitive to any fluctuations in the drive.

Another advantage of the bridge scheme is it's sensitivity. Since it is a null measurement, the differential voltage can be amplified quite a bit without overloading whatever amplifier is being used to measure the voltage (a lock-in amplifier for the ac setup in Figure 3.4). Both features discussed make the wheatstone bridge an optimal setup for noise measurements.

The modified bridge scheme was developed by John Scofield specifically to measure $1/f$ noise in thin films [35]. Instead of using the sample as one of the four resistors in the bridge, the sample is center-tapped and the resulting halves are each used as one resistor in the bridge. Any measured fluctuations away from null will be a result of sample noise (or preamp noise as discussed below). A schematic of the measurement circuit is shown in Figure 3.5.

There are some aspects of this measurement scheme that need addressing. One is that the bridge measurement will be sensitive to fluctuations in not just the sample, but the two variable resistors used to complete the bridge. Thus, choosing these components becomes a critical choice when building the bridge. In this case, two General Radio 1433-H 10 MΩ decade resistors were used. Another important aspect are contact fluctuations (noise in the leads). To solve this problem, Scofield showed that setting the variable resistors to values much higher than the lead resistance will eliminate such issues. Another issue is phase differences between the two sides of the bridge. A phase difference will result in a lower observed noise power than is actually occurring (there will be components of the noise in-phase with the drive current as well as 90 degrees out-of-phase). To solve this,

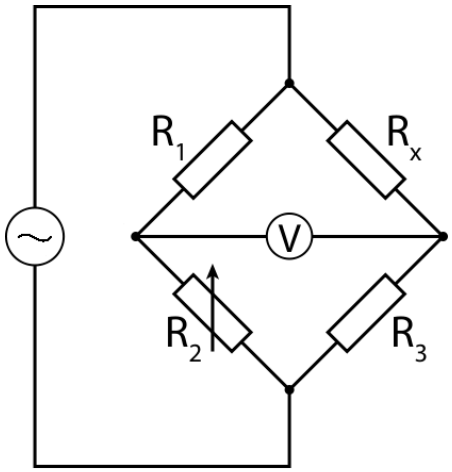

Figure 3.4: A standard Wheatstone bridge. The unknown resistor is R_x. The variable resistor is denoted by the arrow though the resistor.

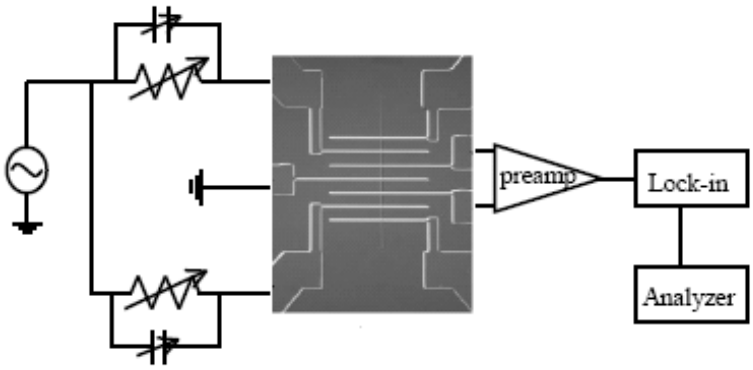

Figure 3.5: The Scofield bridge scheme. The trimming capacitors are used to keep both sides of the bridge in phase.

trimming capacitors were placed on both sides of the bridge. To keep the two sides in phase, the trimming capacitors were altered until the out-of-phase signal was null. The last consideration is the drive frequency to use. The key is to find the lowest possible preamplifier noise associated with the input impedance of the preamplifier. In this case, an NF electronic instruments LI-75A low noise preamplifier was used in combination with drive frequencies near 1 KHz. When the variable resistor values are much larger than the sample resistance, the input impedance seen by the preamplifier should just be equal to the sample resistance.

The ac five-terminal bridge measurement was performed with all the same equipment as the WL magnetoresistance measurement with the addition of the extra preamplifier. The signal from the output of the lock-in amplifier was fed into a Stanford Research Systems SR785 spectrum analyzer. The spectrum analyzer performed a fast Fourier transform (FFT) on the data so it could be observed in the frequency domain. The FFT bandwidth went from 0 to .781-6.25 Hz depending on the size of the noise power.

There is one final measurement detail that has not yet been mentioned. As discussed earlier, there exists extra noise sources (predominantly the preamplifier noise) that must be accounted for in this measurement. By using a lock-in amplifier that can measure both in-phase and 90 degrees out-of-phase simultaneously, the extra noise can be treated quite simply. The trimming capacitors should eliminate any noise from the sample in the out-of-phase channel. Thus, any noise measured in this channel should be preamplifier noise and Johnson noise. The in-phase channel should measure the sample noise plus these extra noise sources. By subtracting the channel 2 noise spectrum from that of channel 1, the resulting noise spectrum should be only the $1/f$ noise from the sample.

An example of the resulting noise power is given in Figure 3.6.

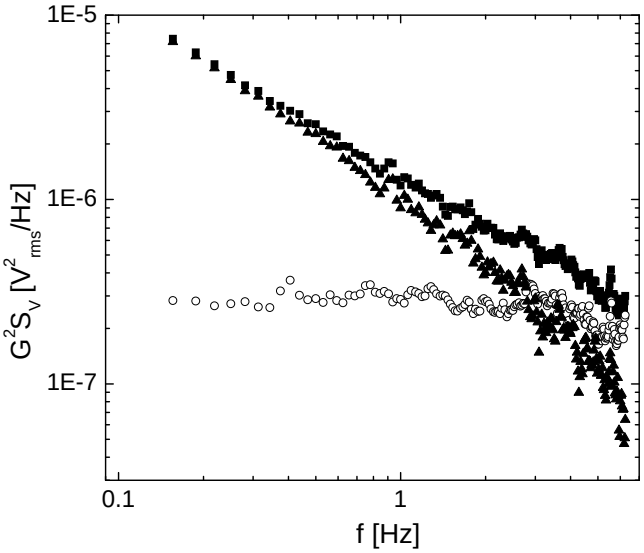

Figure 3.6: A typical noise power spectrum. This data was acquired from a 75 nm wide Au wire. Channel 1 (■), Channel 2(○), and the difference(▲) are all shown. The gain, G, in this measurement was 200,000.

The final noise spectra like the one shown in Figure 3.6 is the result of averaging many spectra acquired one after the next. This averaging was performed in the SR785 spectrum analyzer. As will be discussed in chapter 4, this technique is quite time-consuming.

The ac bridge technique is also an ideal measurement scheme for the magnetofingerprint. If a four-terminal measurement was used to observe MFUCF, all the low field data would be dominated by the WL magnetoresistance. By using the five-terminal setup, this effect is eliminated since each side of the bridge should have an identical WL magnetoresistance. The MFUCF, however, will still be present since each half of the bridge will have a different magnetofingerprint. Thus, the magnetofingerprint can be measured down to zero field with the bridge.

This concludes the dicussion of the necessary background theory and experimental procedures needed to discussed the results and analysis of the experiments performed on the AuPd, Ag, and Au mesoscopic wires.

Chapter 4

Results and Analysis

4.1 AuPd

4.1.1 Results

The goal of the initial measurements using AuPd, first reported in Ref. [36], was to determine the effect of large spin-orbit scattering and large spin-flip scattering on the quantitative consistency between coherence lengths inferred from WL magnetoresistance, L_ϕ^{WL}, and time-dependent universal conductance fluctuations, L_ϕ^{TDUCF}. As explained in Chapter One, the current theory [3] disagreed with the only experimental comparison of L_ϕ^{WL} and L_ϕ^{TDUCF} in Ag films [1]. The only possible explanation offered for the disagreement between the two coherence lengths was due to some, as of yet not understood, effect due to the intermediate spin-orbit scattering in Ag at the temperatures of the measurements. If this was truly the cause, though, then the effect should be even larger in a system with large spin-orbit scattering. This made Au a prime candidate. Due to familiarity working with AuPd [18], this alloy was decided upon as the material to investigate.

The first samples fabricated were 500 nm in width. As will be seen shortly, this puts the samples well into the quasi-2D regime. Once a coherence length scale was determined, samples that fell into the quasi-1D regime were made. The results presented below show data from four samples. The pertinent parameters for each sample are given in Table 4.1. Samples A and B were found to be quasi-1D while C and D were quasi-2D.

Table 4.1: Samples used in magnetotransport and noise measurements. Free electron density of states for Au used to calculate D: 1×10^{47} m^{-3}J^{-1}, from Ref. [9]. Sample D was deliberately contaminated with additional ferromagnetic impurities.

Sample	w [nm]	t [nm]	$R_\square$ [Ω]	D [m^2/s]
A	43	9	32.1	1.34×10^{-3}
B	35	9	31.5	1.34×10^{-3}
C	500	6.5	84.5	7.9×10^{-4}
D	500	8.5	47.9	9.6×10^{-4}

In order to test the effect of spin-flip scattering, sample D was intentionally doped with ferromagnetic permalloy ($Ni_{0.8}Fe_{0.2}$). Doping was accomplished by evaporating ~ 2.5 nm of permalloy with the sample shutter closed prior to evaporating the AuPd.

The first test performed on each sample was an ac four-terminal resistance measurement as a function of temperature at 3 T. This field was high enough to suppress the WL magnetoresistance while leaving the e-e interaction correction to the resistivity unchanged. The test was repeated at multiple drive currents to test for self-heating. Microscopically, self-heating (or Joule heating) results from the energy given to the electrons through the applied electric field. At high temperatures, the electron-electron and electron-phonon interactions are strong allowing the electrons to rethermalize to the bath temperature. If enough energy is given to the electrons at low bath temperatures, however, the poor electron-phonon coupling at these temperatures will not allow the phonons to carry heat away. This leaves only the electrons to dissipate the energy. The electrons are, therefore, at some $T_{eff} > T_{bath}$. This, of course, is highly undesirable as the coherence length is temperature dependent (on the electron's temperature!). By finding the highest drive current that doesn't saturate the upturn in the resistance due to e-e interactions,

the signal-to-noise ratio can be optimized without inhibiting measurements with Joule heating at the lowest temperatures of the experiment.

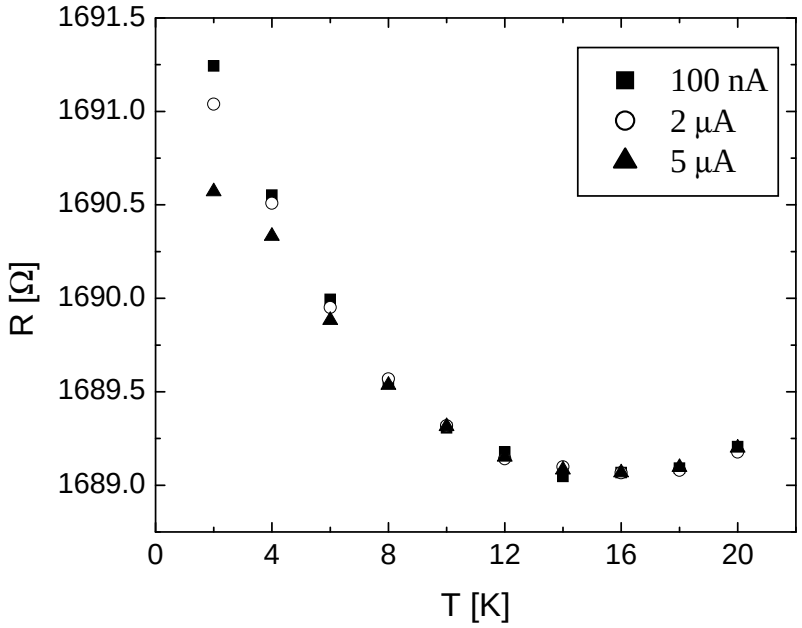

Figure 4.1: Temperature dependence of a 500 nm wide AuPd sample at three different drive currents. By 2 μA, some Joule heating is observed at 6 K.

Once the appropriate drive current was determined, the magnetoresistance was measured. In order to infer the coherence lengths from these measurements, the theoretical functional forms of the magnetoresistance are needed. For quasi-1D and quasi-2D, the fitting functions in the limit of large spin-orbit scattering are [19, 37]:

$$\frac{\Delta R}{R}\Big|_{1\mathrm{d}} = -\frac{e^2}{2\pi\hbar}\frac{R}{L}\left[\frac{1}{L_\phi^2} + \frac{1}{12}\left(\frac{w}{L_\mathrm{B}^2}\right)^2\right]^{-1/2} \tag{4.1.1}$$

$$\frac{\Delta R}{R}\Big|_{2\mathrm{d}} = \frac{e^2}{4\pi^2\hbar}R_\Box\left[\psi\left(\frac{1}{2} + \frac{1}{2}\frac{L_\mathrm{B}^2}{L_\phi^2}\right) - \ln\left(\frac{1}{2}\frac{L_\mathrm{B}^2}{L_\phi^2}\right)\right] \tag{4.1.2}$$

In equation 4.1.1 $\Delta R/R = [R(B) - R(B=\infty)]/R(B=\infty)$ while in equation 4.1.2 $\Delta R/R = [R(B) - R(B=0)]/R(B=0)$. $R_\Box$ is the sheet resistance and w is the sample

width. ψ in equation 4.1.2 is the digamma function. The only unknown parameter in either of these equations is the coherence length, L_ϕ. Thus, it is the only free parameter when fitting the data to the appropriate functional form. In the quasi-1D samples, w is left free when analyzing the 2 K data and left fixed to the 2 K value for all subsequent fits. Finding the width in this manner was in strong agreement with measurements performed via a scanning electron microscope. Figure 4.2 shows the slightly different functional forms of the quasi-1D and quasi-2D magnetoresistance.

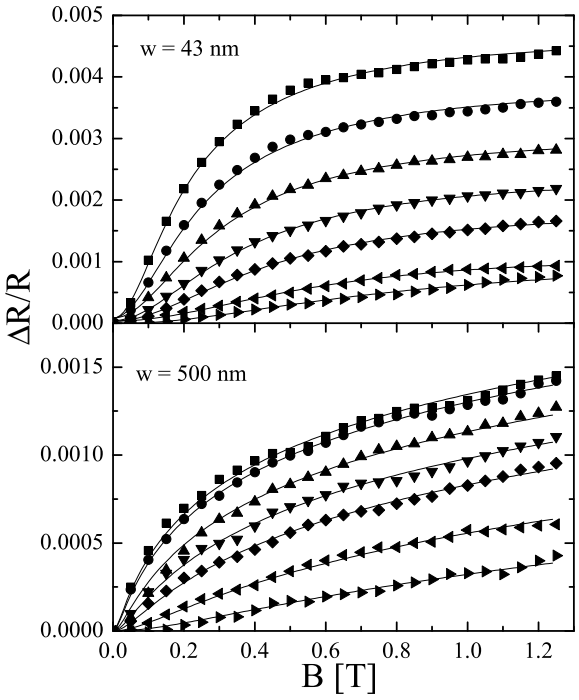

Figure 4.2: The magnetoresistance of a 500 nm (quasi-2D) and 43 nm (quasi-1D) AuPd wire. The qualitative change is the same but the two samples have a slightly different magnetic field dependence.The data is at 2 (■), 4 (●), 6 (▲), 8 (▼), 10 (◆), 14 (◀), and 20 (▶) K

Once the WL magnetoresistance measurements were completed, the measurement

circuit was switched to the ac five-terminal bridge scheme to measure the TDUCF. The measurement of the TDUCF versus magnetic field quickly set the lower bound on how quickly all the necessary measurements could be made on one sample once all the fabrication and measurement techniques were "perfected". While all the magnetoresistance curves for one sample could be acquired in ∼24 hr., the TDUCF took just over ∼24 hr. per temperature! Due to the relatively small size of the TDUCF (with respect to Ag and Au), the TDUCF could be measured only over a very narrow bandwidth. A simple formula can be used to calculate the total time necessary to acquire a noise spectrum is $t = (\Delta f)^{-1} n$ where n is the number of data points in the spectrum (sometimes called FFT lines). This spectrum, however, needs to be measured at least 100 times and then all the resultant spectra are averaged. This all needs to be repeated at each field point. Typically 12 field points were measured. In the case of the AuPd, the bandwidth was at most 1.5625 Hz, meaning the total acquisition time was, at best, 25.6 hrs.

To infer the coherence length from the field-dependence of the TDUCF was quite a bit more trouble than the WL inference. As the quasi-2D analysis was being performed, the only known fitting function had no analytic form. The numerical form was explained in detail in Ref. [26]. To perform the fit numerically, a 3D array (the variables were, B, L_ϕ, and $L_{\rm th}$) of values were calculated and used to build an interpolating function. This interpolating function could then be used as the quasi-2D crossover function. Soon after the quasi-2D data analysis was completed an analytic form of the large spin-orbit scattering quasi-2D crossover function was found [38]. In the absence of a magnetic field

parallel to the plane of the sample, this form of the crossover function has the form:

$$\nu_{2d}(B) = \frac{1}{2} + \frac{L_B^2}{4L_\phi^2}\psi'\left(\frac{1}{2} + \frac{L_B^2}{2L_\phi^2}\right) \tag{4.1.3}$$

where ψ' is the derivative of the digamma function. Inferring coherence length information from both the numerical crossover function and the analytic crossover function differed by only 3-4 %. Strictly speaking, equation 4.1.3 is only valid when $\hbar/\tau_\phi << k_B T$ which is not the case in this system. The small difference in the resulting coherence lengths, however, suggests that the equation is robust even when the high thermal energy limit is not met.

The quasi-1D noise crossover data was a bit less trouble to fit. In this dimensionality, an approximate magnetic field correlation function was calculated [39]. This could then be used to calculate the crossover function using the same procedure laid out in Ref. [32]. A comparison between the TDUCF and MFUCF, which was explained in detail in Chapter Three, showed the TDUCF to be deep into the unsaturated regime (the number of decades to integrate over was ∼300). Thus, the crossover function should be related to the derivative of the field correlation function with respect to the dephasing rate. The resulting derivative is:

$$F'(B) = \frac{L_{\phi B}^5\left(1 + \frac{3L_{\phi B}^2(B)}{2\pi L_{th}^2}\right)}{\left(1 + \frac{9L_{\phi B}^2(B)}{2\pi L_{th}^2}\right)^2} \tag{4.1.4}$$

where

$$L_{\phi B}^2(B) = \frac{3L_\phi^2}{(BeL_\phi w/\hbar)^2 + 3}. \tag{4.1.5}$$

Of course, this is just the cooperon contribution to the correlation function. The crossover

function should be:

$$\nu_{1d}(B) = \frac{1}{2} + \frac{F'(B)}{2F'(B=0)}. \tag{4.1.6}$$

The 1/2 factor comes from the diffuson contribution to the correlation function.

An exact analytic form for the quasi-1D, large spin-orbit interaction crossover function was also given in ref. [38]. It has the form:

$$\nu_{1d}(B) = 1 - \frac{x}{2}\left(\frac{Ai(x)}{Ai'(x)}\right)^2 \tag{4.1.7}$$

where $x \equiv L_\phi^2/(3(\hbar/Bew)^2)$. In this case, the two fitting functions result in inferred coherence lengths that differ by roughly 13 %. An example of the noise crossover is given in Figure 4.3.

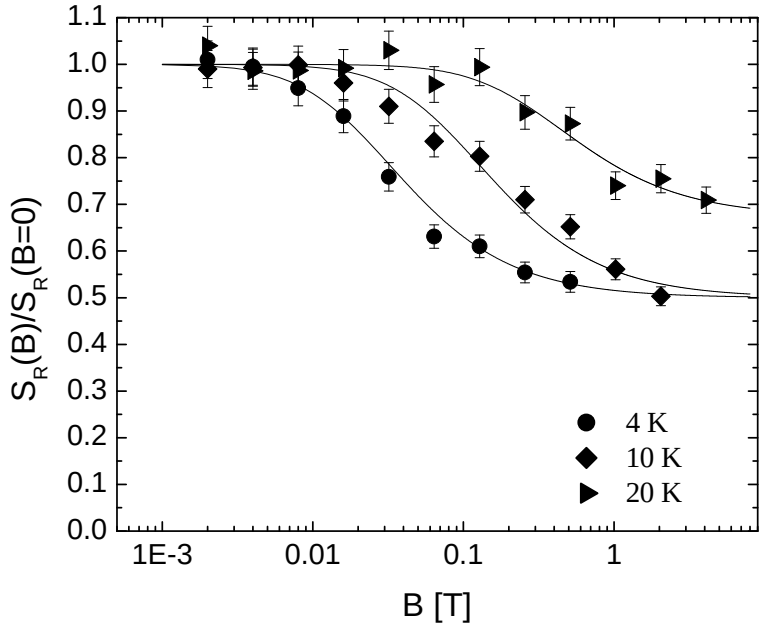

Figure 4.3: The magnetoresistance of a 500 nm (quasi-2D). The 20 K data fails to drop by a full factor of 2 due to classical local interference noise.

Figure 4.3 has one important detail that warrants further discussion. At 20 K, the

noise power does not decrease by a full factor of 2. This is easily explained. Once the temperature gets high enough, the classical local interference noise contribution to the total $1/f$ in the sample becomes non-negligible. This local interference noise certainly should not decrease with an applied magnetic field. Thus, the total measured noise will not decrease by a full factor of 2. When this occurs, a second parameter needs to be added to the fitting function. In this case, the fitting function becomes:

$$f(B) = c\nu(B) + (1 - c) \tag{4.1.8}$$

where the parameter c is the fraction of the noise due to quantum interference.

Before discussing the coherence length results, one last result of the TDUCF measurement needs to be mentioned. The magnetic field dependence of the TDUCF shows a very interesting effect above .5 T in the AuPd samples. A large upturn in the noise is observed in all the samples. The sample intentionally doped with magnetic impurities showed the greatest upturn, though. An example is shown in Figure 4.4.

This same effect was observed in TDUCF measurements on Li wires [17]. The upturn is a result of the presence of paramagnetic impurities in the system. The magnetic impurities cause spin-flip scattering that reduces the coherence length and, thus, the size of the TDUCF noise power. By applying a magnetic field, the spin states of the impurities begin to split. When these states differ in energy by more than $k_{\mathrm{B}}T$, the spin of each impurity should align. This, in effect, turns off the spin-flip scattering and the TDUCF noise power should increase due to the now larger coherence length.

Figure 4.5 shows the inferred coherence lengths from both the WL magnetoresistance and the magnetic field dependence of the TDUCF. The results are unequivocal. In all

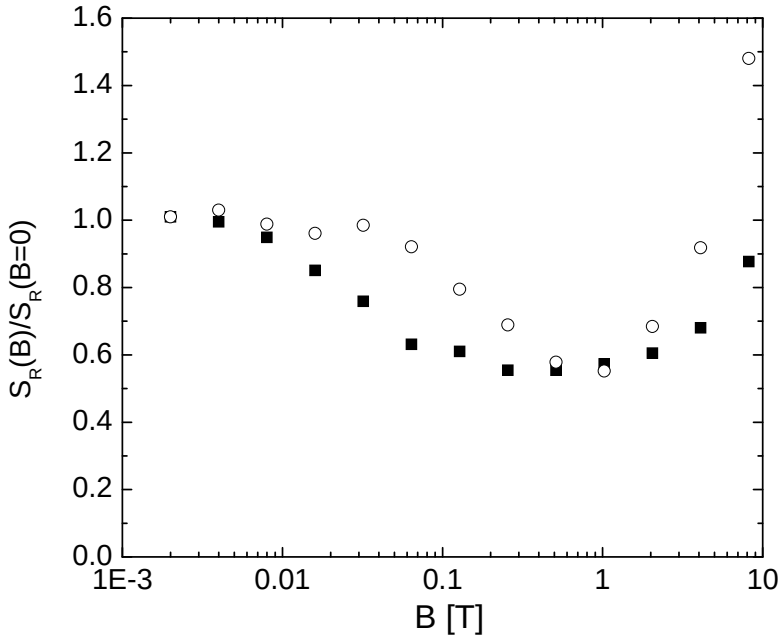

Figure 4.4: The normalized noise power as a function of magnetic field up to 8.12 T. The data are for samples C (■) and D (○) at 4 K. The large upturn is attributed to Zeeman splitting of paramagnetic impurities in the AuPd.

four samples the inferred coherence lengths are in excellent quantitative agreement. In fact, even in sample D, in which a large amount of paramagnetic impurities exist, the lengths are still in excellent agreement.

4.1.2 Analysis

The temperature dependence of the coherence lengths shows gives a wealth of information. For example, the electron-phonon scattering seems to be the dominant dephasing mechanism above 6 K. This is inferred from the steeper decrease in the coherence length above this temperature. Another important fact to note is how far below the Nyquist scattering length the inferred coherence lengths sit. The most likely reason for this is the magnetic impurities that are present even in the "nominally" clean samples. These

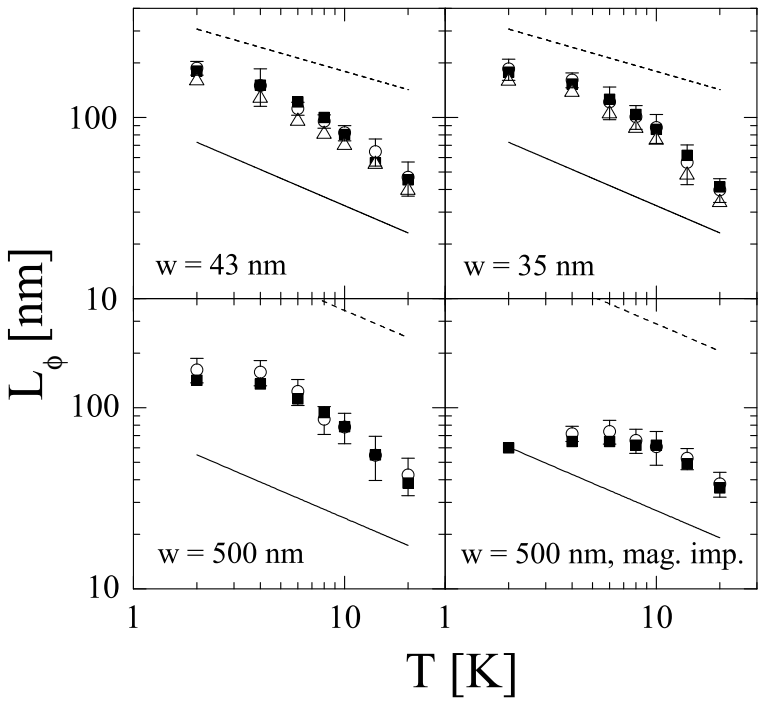

Figure 4.5: L_ϕ^{WL} and L_ϕ^{TDUCF} for all four samples measured. The dotted line is the predicted Nyquist dephasing length and the solid line is the thermal length. Both lengths were calculated using the sample parameters from Table 4.1. In the two quasi-1D samples L_ϕ^{WL} is (■), Aleiner L_ϕ^{TDUCF} is (△) and Beenakker/van Houten L_ϕ^{TDUCF} is (○). In the two quasi-2D samples L_ϕ^{WL} is (■) and L_ϕ^{TDUCF} is (○).

impurities introduce an extra dephasing mechanism which would lower the overall coherence length. The final behavior to note is the apparent saturation of sample D. There seems to be ample evidence in this case that the saturation is the result of an increased concentration of magnetic impurities.

The apparent coherence saturation at low temperature caused by magnetic impurities is actually not a true saturation. The concept is explained in detail in Ref. [19]. Equation 1.3.6 expressed how the different dephasing mechanisms add. This equation, though, is only correct when $\tau_{\mathrm{sf}} > \tau_{\mathrm{K}}$ where τ_{K} is the spin-relaxation time (known as the Korringa

time). This inequality is true if $T \gtrsim c_{\mathrm{mag}}/\nu(E_{\mathrm{F}})(k_{\mathrm{B}}$. When the temperature is above the necessary value, the spin-flip scattering time is given by the Nagaoka-Suhl formula [40]:

$$\frac{1}{\tau_{\mathrm{sf}}} = \frac{c_{\mathrm{mag}}}{\pi\hbar\nu(E_{\mathrm{F}})} \frac{\pi^2 S(S+1)}{\pi^2 S(S+1) + \ln^2(T/T_{\mathrm{K}})}, \tag{4.1.9}$$

where $\nu(E_{\mathrm{F}})$ is the density of states at the Fermi level of the host metal, S is the spin of the impurity, and T_{K} is the Kondo temperature of the impurity in the host metal. This means that as the temperature decreases, τ_{sf}^{-1} will increase while $\tau_{\mathrm{e\text{-}e}}^{-1}$ will decrease. The net effect is a roughly temperature independent dephasing rate. This "plateau" in the coherence length disappears when $T \leq T_{\mathrm{K}}$.

Equation 4.1.9 can be used to estimate the magnetic impurity concentration required to produce the observed L_ϕ saturation values. Assuming that the 2 K data represent complete saturation (as appears to be the case for sample C), and that $T_{\mathrm{K}} \sim 2$ K, and a typical $\nu(E_{\mathrm{F}})$ for the noble metals, the c_{mag} is found to be ∼17 ppm for sample C. This value is surprisingly high and not consistent with the starting purity of the source material. A possible explanation for this would be an enhancement of the spin-flip scattering due to the strong paramagnetism of the Pd in this alloy. Note that even if this concentration of magnetic impurities is correct, the inferred T^* below which equation 1.3.6 no longer holds is < 1 K, well below the temperatures of these measurements.

Comparing the saturated values of L_ϕ for two samples allows the relative concentrations of magnetic impurities to be computed, independent of possible paramagnetic enhancement or density of states uncertainties, since $\frac{c_{\mathrm{mag},2}}{c_{\mathrm{mag},1}} = \frac{D_2}{D_1}\left(\frac{L_{\phi,1}}{L_{\phi,2}}\right)^2$. Comparing sample C (quasi-2d) and D (quasi-2d, doped with additional magnetic impurities), the ratio $c_{\mathrm{mag,D}}/c_{\mathrm{mag,\ C}} \approx 5$. The $R(T)$ curves for these two samples show no discernable

difference beyond what would be expected from their diffusion constants. This also supports the hypothesis that the absolute concentration above is an overestimate, since $\sim$ 100 ppm magnetic impurities in sample D would likely cause other discernable effects (like hysteresis and/or spin glass signatures like aging) in addition to enhanced dephasing. Furthermore, at such a concentration the crossover temperature $T^* \sim 4$ K. Once equation 1.3.6 is no longer valid, the spin-flip scattering affects WL and TDUCF differently which, in turn, should result in different coherence lengths for the two measurements. The strong agreement in sample D implies that the magnetic impurity concentration is less than the estimate.

The most telling result of the four samples is the strong quantitative agreement between the coherence lengths inferred via WL and TDUCF. This supports the claim that these two phenomena probe precisely the same physics [3]. The result, however, is in severe disagreement with the results of Ref. [1]. The AuPd results combined with those seen previously in Ag films seem to eliminate a spin-orbit effect as the cause of coherence length disagreement seen in Ag. The Ag results show a divergence of the two inferred coherence length below 10 K. As the temperature is lowered, the Ag moves closer and closer to the large spin-orbit regime. If the spin-orbit scattering is the relevant physics, the AuPd should behave like the low temperature limiting behavior of the Ag. In order for the two results to be consistent, the coherence length divergence in the Ag would have to stop at some low temperature and then the two values would have to converge again. This seems highly unlikely.

It would appear, then, that a different explanation for the coherence length disagreement in the Ag data is necessary. To determine the explanation, revisiting the coherence

length comparison in Ag is necessary to eliminate experimental flaws in the previous Ag experiment as the cause of the disagreement. Problems such as Joule heating during the TDUCF measurement was already shown not to be the culprit, but external dephasing mechanisms such as microwave electromagnetic noise broadcast down to the sample may be an issue [41]. Since the measurement schemes for WL magnetoresistance and TDUCF versus magnetic field are different, such an issue may have affected the samples differently in the two measurements. By repeating the measurements with a slightly different measurement scheme and in a different location, it would seem highly unlikely to recover the same results if the coherence length divergence in Ag was caused by a mechanism such as microwave electromagnetic noise. Also, by repeating the measurement in quasi-1D samples, such an effect may be increased due to an increased inability to dissipate the heat associated with such a noise.

4.2 Ag

4.2.1 Results

The experiments using Ag were initially started to determine the reproducibility of the previous coherence length comparisons done in Ag films. The results were initially reported in Ref. [42]. However, the system provided insight into other interesting aspects of quantum transport phenomena. One interesting observation was self-averaging due to high drive currents (this was discussed in the Averaging Effects section of chapter 3).

The only difference in the fabrication of the Ag was eliminating using Ti/Au leads. Thus, fabrication only required one lithography step. The important sample parameters of all the Ag samples investigated are given in Table 4.2. The data acquisition was

Table 4.2: Samples used in magnetotransport and noise measurements. Free electron density of states for Ag was used to calculate D. The effective dimensionality d for coherence effects is determined by the relative size of L_ϕ and the sample dimensions.

Sample	metal	w [nm]	t [nm]	R/L [Ω/μm]	D [m^2/s]
E	Ag	115	12	49	5.65 $\times 10^{-3}$
F	Ag	140	12	35	6.70 $\times 10^{-3}$
G	Ag	130	12	45	5.63 $\times 10^{-3}$
H	Ag	70	20	42	6.50 $\times 10^{-3}$
I	Ag	125	12	43	5.91 $\times 10^{-3}$
J	Ag	100	12	88.5	3.61 $\times 10^{-3}$

performed in exactly the same manner as the AuPd data.

To fit the WL magnetoresistance, a more general form of equation 4.1.1 was necessary so as to account for intermediate spin-orbit scattering. This form of the equation takes the form [19]:

$$\frac{\Delta R}{R}\Big|_{1\mathrm{d}} = -\frac{e^2}{2\pi\hbar}\frac{R}{L}\left[3\left(\frac{1}{L_\phi^2}+\frac{4}{3L_{\mathrm{so}}^2}+\frac{1}{12}\left(\frac{w}{L_{\mathrm{B}}^2}\right)^2\right)^{-1/2}-\left(\frac{1}{L_\phi^2}+\frac{1}{12}\left(\frac{w}{L_{\mathrm{B}}^2}\right)^2\right)^{-1/2}\right] \tag{4.2.1}$$

Notice when $L_{\mathrm{so}} \ll L_\phi$, the first bracketed term becomes very small and equation 4.1.1 is recovered. The spin-orbit scattering length was left as a free parameter at 2,4, and 6 K. The values were then averaged and used for all subsequent fits. A typical spin-orbit scattering length in the Ag samples was ∼300 nm.

The crossover function has a similar result. Equation 4.1.4 can be modified per the explanation in ref. [14]. The correlation function derivative becomes:

$$F'(B) = \frac{L_{\phi\mathrm{B}}^5\left(1+\frac{3L_{\phi\mathrm{B}}^2(B)}{2\pi L_{\mathrm{th}}^2}\right)}{4\left(1+\frac{9L_{\phi\mathrm{B}}^2(B)}{2\pi L_{\mathrm{th}}^2}\right)^2}+\frac{3L_{\phi\mathrm{Bt}}^5\left(1+\frac{3L_{\phi\mathrm{Bt}}^2(B)}{2\pi L_{\mathrm{th}}^2}\right)}{4\left(1+\frac{9L_{\phi\mathrm{Bt}}^2(B)}{2\pi L_{\mathrm{th}}^2}\right)^2} \tag{4.2.2}$$

where

$$L^2_{\phi \mathrm{Bt}}(B) = \frac{3L^2_\phi L^2_{\mathrm{so}}}{(BeL_\phi L_{\mathrm{so}} w/\hbar)^2 + 3L^2_{\mathrm{so}} + 4L^2_\phi}. \tag{4.2.3}$$

Again, in the limit of strong spin-orbit scattering, the term involving the spin-orbit scattering becomes small and equation 4.1.4 is recovered (there is an extra factor of 4, but it is irrelevant for the crossover function).

A typical WL magnetoresistance is shown in Figure 2.6. Examples of the noise crossover function is given in Figure 4.6.

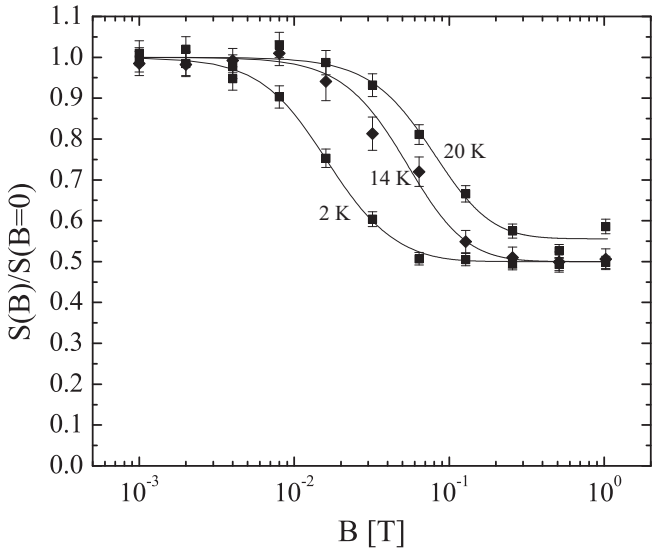

Figure 4.6: The noise crossover at 2, 14, and 20 K in sample E. Again, the 20 K data does not decrease by a full factor of 2.

The coherence lengths inferred from sample F are shown in Figure 4.7. The dashed line is the Nyquist scattering length and the solid line is the thermal length of the sample.

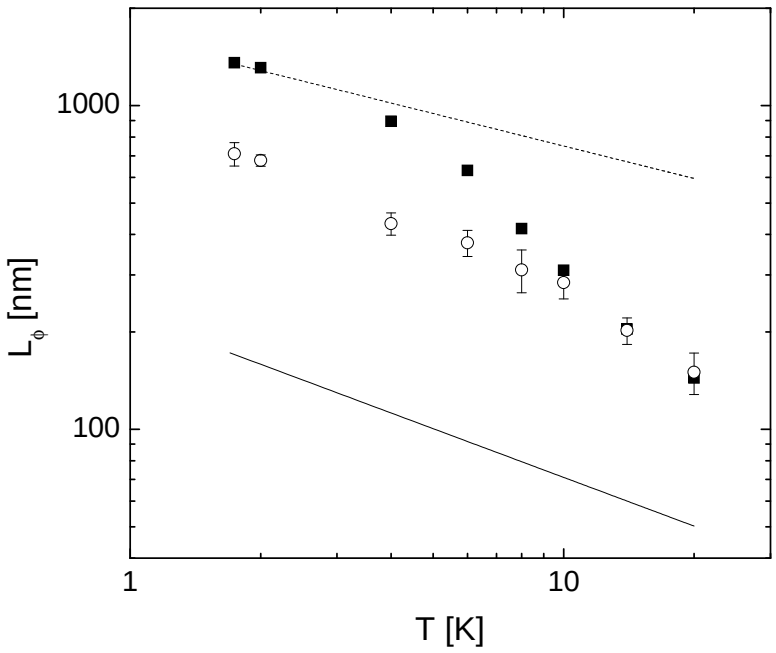

Figure 4.7: Coherence lengths inferred for sample F. A distinct divergence between L_ϕ^{WL} (■) and L_ϕ^{TDUCF} (○) below 10 K.

4.2.2 Analysis

The resulting coherence lengths are quite striking. Just as reported in ref. [1], there is an obvious disagreement between L_ϕ^{WL} and L_ϕ^{TDUCF} below a critical temperature (∼10 K in this case). The fact that the results are almost identical to the quasi-2D results is a strong indicator that external dephasing mechanisms are not causing the divergence. Also, the fact that no divergence is seen in the AuPd results would also seem to argue against an extrinsic cause for this discrepancy. Finally, no heating is observed at the lowest measured temperatures when very low currents are used to measure the $R(T)$ of the samples. All signs seem to indicate that the discrepancy is real, not a cause of some external dephasing mechanism affecting the two measurements differently.

Before discussing other possible explanations for the coherence length disagreement, one other aspect of the resulting L_ϕ^{WL} is worth noting. The values at the lowest temperatures are in strong agreement with the Nyquist scattering length. This would suggest that the Ag has a very small concentration of magnetic impurities, if any. This is supported by the TDUCF noise power at high magnetic field. Unlike the AuPd, the noise power shows no discernable upturn. An example is shown in Figure 4.8.

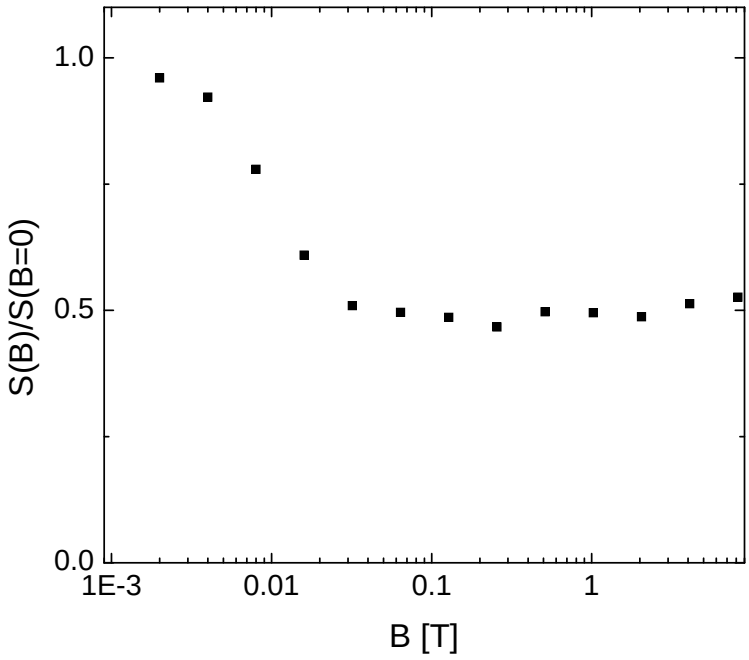

Figure 4.8: The noise crossover at 2 K for sample F. There is no noticeable upturn in at high field suggesting that the magnetic impurity concentration is much lower than the AuPd samples.

Coherence saturation was observed in sample G and H which were measured below 2 K using a ^{3}He/^{4}He dilution refrigerator. The noise could not be measured at such low temperatures due to Joule heating. Without this measurement it is hard to attribute the

Table 4.3: $L_\phi^{\mathrm{WL}}(\max)$ normalized by that for sample H, compared with the expected ratio from equation 4.2.4 for zero-temperature saturation of τ_ϕ, using sample parameters from Tables 4.1 and 4.2.

Sample ratio	Measured	Uncertainty	Expected
C/H	0.0597	0.0017	0.0148
D/H	0.0221	0.0006	0.0218
G/H	0.6561	0.0186	0.7502

saturation to magnetic impurities. An alternative explanation for low temperature coherence saturation suggests neglected interaction effects of electrons can cause dephasing analogous to the dephasing caused by the e-e interactions related to thermal noise [5]. This dephasing is constant all the way to $T = 0$. The predicted zero-temperature dephasing time is

$$\frac{1}{\tau_{\phi,\mathrm{sat}}} = \frac{\sqrt{2}\rho e^2}{3h\pi\sqrt{D}} \left(\frac{b}{\tau}\right)^{3/2} \tag{4.2.4}$$

where τ is the elastic relaxation time of the conduction electrons, ρ is the resistivity, and b is a constant of order one. Since a strict value of b is not known, sample H was chosen as a reference and compared to other samples showing coherence saturation. By calculating the ratio of two saturated coherence times, the dependence on the unknown parameter b is eliminated. Table 4.3 shows the theoretical and experimental results of comparing the saturated coherence lengths of samples G, C, and D (C and D were AuPd). Only one of the three comparisons show agreement between the theoretical and experimental ratios and that is sample D, the sample known to have a high concentration of magnetic impurities. It has been shown that even very small concentrations of magnetic impurities can result in coherence saturation [7] and this is the likely explanation for the saturation seen in samples G and H.

Returning to the coherence length divergence: a possible explanation for the coherence length disagreement in Ag comes from the fact that the WL and TDUCF measurements were done at different drive currents. Due to signal-to-noise difficulties, the TDUCF measurements were always done at larger currents than the WL measurements. The TDUCF noise power showed a strong drive current dependence around these drive currents without showing any $R(T)$ saturation. The most likely cause of this strong dependence is averaging due to $eV_\phi > E_c$. It has been suggested, however, that the system is in a non-equilibrium limit where extra dephasing can occur without an observable change in the $R(T)$ [43]. Thus, this must be investigated as an explanation for the observed divergence between the coherence length inferences.

To check the possible non-equilibrium effect on L_ϕ^{TDUCF}, the TDUCF crossover was measured at three different currents. While the normalized noise power showed a clear decrease, the noise crossover field showed no change. The results are shown in Figure 4.9. The results are unmistakable. The noise power shows a strong drive dependence, but the corresponding noise crossover field remains unchanged. It would appear that non-equilibrium dephasing is not the cause of the coherence length divergence. For completeness, a rigorous noise power versus drive current test was performed at multiple temperatures to determine if the drive dependence of the TDUCF is truly an averaging effect. The results are shown in Figure 4.10.

These results leave little doubt the drive dependence is an averaging effect. Two features of the results are telltale signs. One is the fact the noise power does not decrease until a certain drive is reached. This point is likely when the voltage across a coherent volume is larger than the Thouless energy. The other sign is that the critical drive

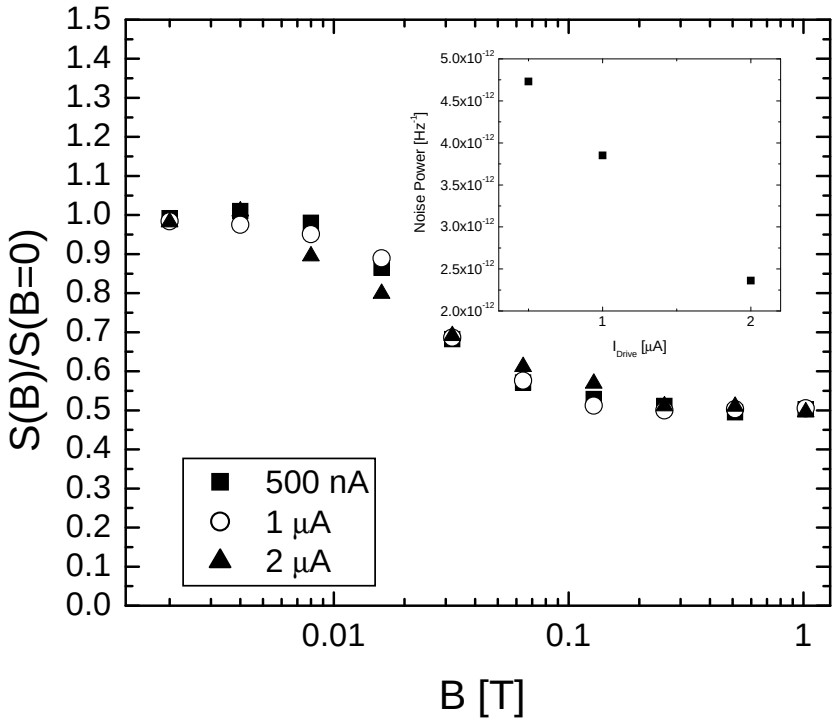

Figure 4.9: The noise crossover at 2 K in sample J at three drive currents, 500 nA, 1 μA, and 2 μA. The inset shows the corresponding normalized noise power for all three drive currents. The noise power amplitude shows a clear drive dependence while the crossover field is unchanged.

changes with temperature. Again, this reflects the change in the Thouless energy due to the temperature dependence of the coherence length.

The possible explanations for the disagreement between L_ϕ^{WL} and L_ϕ^{TDUCF} are quickly being eliminated. One possible explanation has not yet been considered; the experimentalists have incorrectly analyzed the data. The theory explaining both WL and TDUCF is well established and the quantitative agreement in the coherence lengths seen in the AuPd suggest that the fitting functions used to analyze the data are not flawed. There is one possible issue though. The Ag TDUCF, like the AuPd TDUCF, were assumed to be

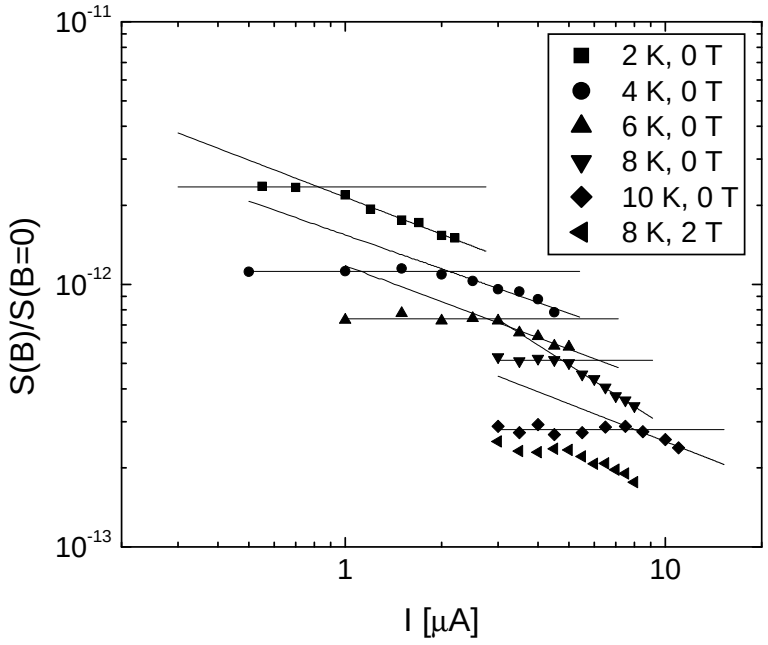

Figure 4.10: The drive dependence of sample E at 2, 4, 6, 8, and 10 K. The characteristic current needed to lower the noise amplitude changes with temperature, indicating an averaging related to the Thouless energy is the cause. The measurement at 8 K and 2 T shows that the coherence length has no strong dependence on field (no spin-flip scattering). The lines are a guide for the eye.

deep in the unsaturated regime. This seemed reasonable as the TDUCF/MFUCF comparison showed that an integration of the TDUCF over ∼240 decades would be needed to recover the MFUCF variance. However, an analysis of the TDUCF crossover data using the saturated crossover function is worth trying. In the saturated case, the correlation function is used instead of its derivative. Using the Beenakker/van Houten results, the correlation function in the absence of spin-orbit scattering is:

$$F(B) \propto \frac{L_{\phi \mathrm{B}}^3}{1 + \frac{9L_{\phi \mathrm{B}}^2(B)}{2\pi L_{\mathrm{th}}^2}} \tag{4.2.5}$$

As explained earlier, the spin-orbit scattering must be considered, resulting in a modified

correlation function:

$$F(B) \propto \frac{L_{\phi \mathrm{B}}^3}{4\left(1+\frac{9L_{\phi \mathrm{B}}^2(B)}{2\pi L_{\mathrm{th}}^2}\right)} + \frac{3L_{\phi \mathrm{Bt}}^3}{4\left(1+\frac{9L_{\phi \mathrm{Bt}}^2(B)}{2\pi L_{\mathrm{th}}^2}\right)} \tag{4.2.6}$$

where $L_{\phi \mathrm{B}}$ and $L_{\phi \mathrm{Bt}}$ are both the same as earlier defined.

When the noise crossover data is analyzed using the saturated crossover function the resulting coherence lengths are in strong disagreement with L_ϕ^{WL}. However, as the temperature decreases, the saturated L_ϕ^{TDUCF} and L_ϕ^{WL} start to converge. The results are shown in Figure 4.11.

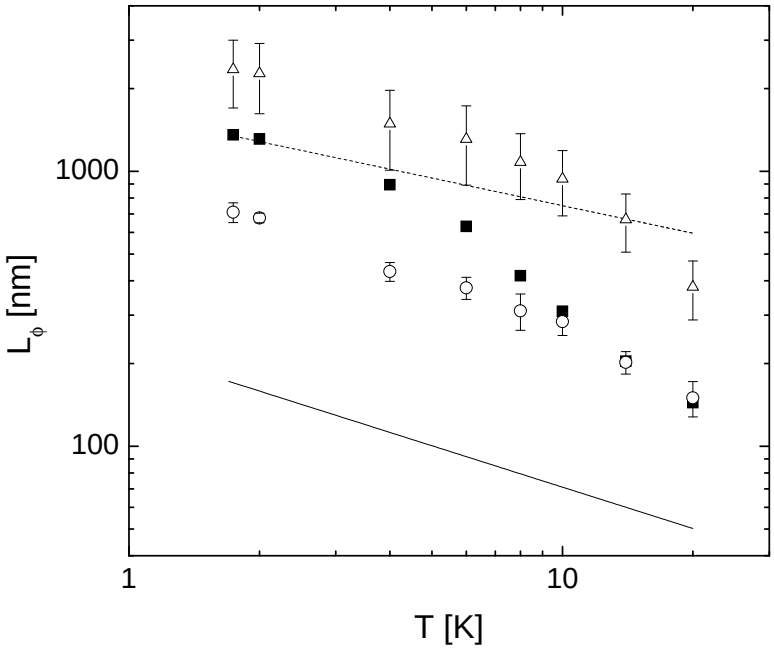

Figure 4.11: Coherence lengths inferred for sample F. L_ϕ^{WL} (■), unsaturated L_ϕ^{TDUCF} (○), and saturated L_ϕ^{TDUCF} (△) are all shown.

The results are suggestive that the TDUCF may be in an intermediate region when neither the unsaturated nor the saturated crossover functions are appropriate. That such a case may exist should not be surprising. The two cases reported assume either very

small impurity potential changes due to mobile TLS or very large impurity potential changes. There does not seem to be a physical reason why a weakly disordered metal should always exhibit impurity potential fluctuations in either of these limits. Also, the fact the TDUCF/MFUCF comparison gave a smaller necessary bandwidth to integrate the Ag noise over than the AuPd would support the data that the AuPd is deeper in the unsaturated regime while the Ag is closer to the saturated regime.

If a transition between regimes is truly occurring in the Ag samples as the temperature is cooled, why such a change should occur needs an explanation. Although the number of mobile TLS should decrease as the temperature decreases, each TLS becomes much more effective at changing the quantum interference. This would imply that one impurity should effect the change in the impurity potential more. As long as the effectiveness of each TLS has a stronger temperature dependence than the concentration of TLS, then the TDUCF should more farther into the saturated regime as the temperature is reduced.

There is an interesting way to try and test whether such a crossover is occurring. If the thermal averaging and drive current averaging are accounted for, looking at the noise power as a function of temperature should show whether such a crossover is occurring. The thermal averaging can be accounted for by dividing the noise power by L_{th}^2. The drive current averaging can be ignored if a low enough drive current is used at each temperature. Fortunately, all the necessary data already exists in Figure 4.10. The result of the analysis is shown in Figure 4.12.

The data in Figure 4.12 indicate that the TDUCF should indeed be approaching the saturated regime with decreasing temperature. The steepness of the corrected noise power at higher temperatures is reflective of the stronger temperature dependence of the

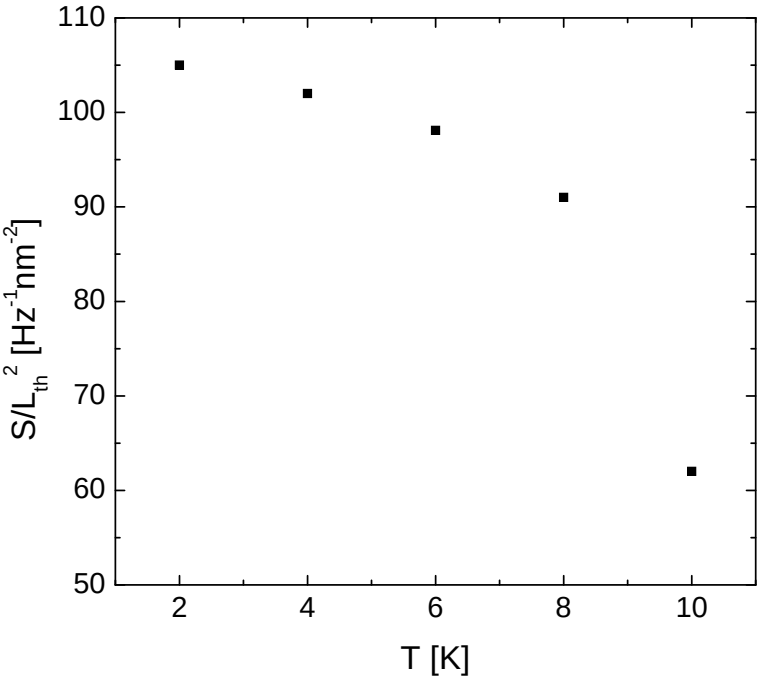

Figure 4.12: The noise power of sample F corrected for thermal averaging. This value increasing as the temperature is lowered indicates the system is moving closer to the saturated TDUCF regime.

coherence length at this temperature due to electron-phonon interactions.

The saturated/unsaturated hypothesis cannot be eliminated with the Ag results. It has, by no means, been proven correct either. Ideally, the best way to confirm this hypothesis would be to continue the coherence length comparison to lower temperatures and see if saturated L_ϕ^{TDUCF} and L_ϕ^{WL} converge and then show quantitative agreement below the convergence temperature. This, however, does not seem possible with current experimental equipment. The difficulty arises from Joule heating. The noise power does not grow quickly enough as the temperature is lowered. Below $\sim$1 K the largest drive currents that don't result in Joule heating are too low to lift the $1/f$ noise out of the background noise floor.

Two other tests could help prove the validity of this hypothesis. One would be to modify the coherence length of the system without greatly changing the number of TLS causing the TDUCF. If the coherence length is reduced, for instance, then it would not be surprising to see the unsaturated crossover function give a coherence length in better agreement with the WL result. The other would be to modify the TLS concentration while leaving the coherence length unchanged. In this case, if the TLS concentration was reduced, again the system should move deeper into the unsaturated TDUCF regime.

As well as developing experimental techniques to attempt the two tests mentioned above, it would also be prudent to perform the coherence length comparison in another normal metal with long coherence lengths to see if results similar to Ag are observed. This was the next experiment performed, using very pure Au.

4.3 Au

4.3.1 Results

All the experiments with Au were performed with source material rated as 99.9999 % pure. For reasons to be discussed shortly, a Ti adhesion layer was used in only certain samples. The samples were all ∼70 nm wide. The data acquisition schemes were the same as for the AuPd and Ag. Since Au is a large spin-orbit scattering material, the fitting functions given in the AuPd section were also used to analyze the Au data. An example of the WL magnetoresistance is given in Figure 2.8. A typical TDUCF crossover data set is shown in Figure 4.13.

In the absence of the Ti adhesion layer, the high field noise crossover data showed no

upturn. As with the Ag, this result was interpreted as indicating a very small concentration of magnetic impurities in the Au. However, a large upturn was observed when a Ti adhesion layer was used. Figure 4.14 shows the difference in the high field crossover data between no Ti present and a 1 nm thick adhesion layer of Ti.

The most interesting characteristic of the magnetic behavior seen with the Ti is that continued exposure to air reduced the magnetic signature significantly. An example of L_ϕ^{WL} before extended exposure to air and after roughly two weeks in air is given in Figure 4.15. A complete discussion of this effect is presented in appendix 1.

The fact that the magnetic signal can be suppressed through exposure to air provides the means to alter the coherence length of a Au nanowire while not drastically effecting the TLS contributing to the TDUCF. This is, as mentioned earlier, one way to try and test the saturated/unsaturated TDUCF hypothesis. The data also show how powerful a tool both the TDUCF and WL magnetoresistance measurements can be in detecting magnetic signatures. This idea was suggested and experimentally proven successful [44].

The other test of the saturated/unsaturated hypothesis is to try and lower the TLS concentration while not altering the coherence length. While attempting an experiment to observe Kondo physics with a molecule studied by other members of the lab [45] an interesting observation was made. After self-assembly of the molecule, the TDUCF noise power was reduced by close to a factor of 2. In order to test whether the effect was caused by just assembling a molecule on the surface of the Au, a simple alkanethiol molecule was used instead of the transition metal coordination complex molecule. To perform the test, a neat solution of dodecanethiol ($CH_2(CH_3)_{11}SH$) was diluted to .1 mM in ethanol. After performing the necessary WL and TDUCF measurements without the SAM, the

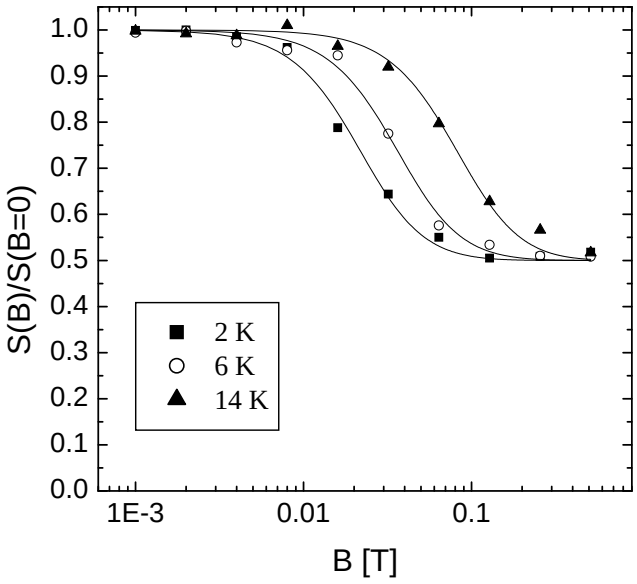

Figure 4.13: The TDUCF crossover of a 70 nm wide Au sample with no Ti adhesion layer. The fits used correspond to the unsaturated crossover function.

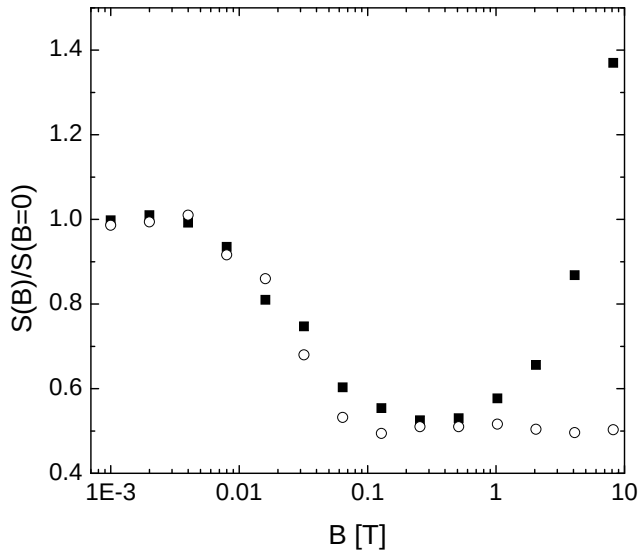

Figure 4.14: The full noise crossover data for a sample with a 1 nm Ti adhesion layer (■) and without an adhesion layer of any kind (○).

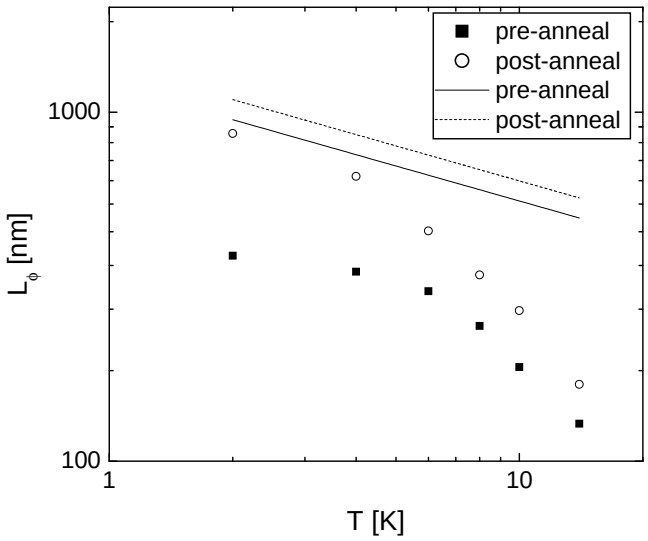

Figure 4.15: The coherence length comparison for an 80 nm wide Au wire before (top) and after (bottom) extended exposure to ambient lab conditions.

sample of interest was removed from the cryostat and soaked in the diluted solution for 48 hours. The same measurements were then repeated with all the same drive currents. The results of the noise power comparison with and without the dodecanethiol SAM is shown in Figure 4.16.

As long as the SAM assembly does not change the coherence length of the system, a dodecanethiol SAM provides the other tool needed to test the saturated/unsaturated TDUCF hypothesis. An example of L_ϕ^{WL} is shown before and after SAM assembly on a 70 nm wide Au sample in Figure 4.17. The results show almost no change in the coherence length inferred from the WL magnetoresistance. Thus, the SAM procedure should indeed provide the method for changing the TLS concentration without modifying the coherence physics. Results of the coherence length comparison both before and after dodecanethiol assembly are given in Figure 4.18.

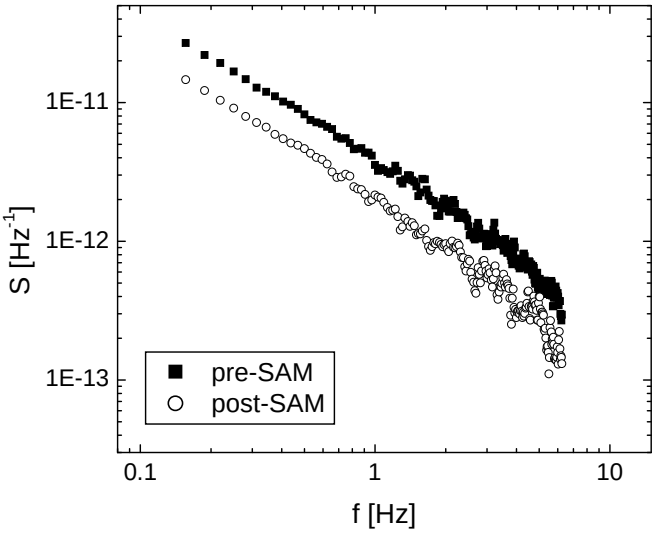

Figure 4.16: The normalized noise power of a 60 nm wide Au sample without a Ti adhesion layer. The noise power is shown both before and after SAM assembly.

4.3.2 Analysis

The Ti/Au results alone tell a compelling story, but coupled with the results from the Au/SAM experiments, there is little doubt what is causing the disagreement between L_ϕ^{WL} and L_ϕ^{TDUCF} in Au and most likely Ag. A series of observations between the experiments leads to the conclusion that a saturated/unsaturated crossover is indeed the cause of the disagreement.

The first observation is that L_ϕ^{TDUCF} shows little to no change before and after air exposure in the Ti/Au experiment. However, the TDUCF noise power shows a distinct increase after the extended air exposure. The change in normalized noise power is shown in Figure 4.19. The noise power after air exposure was corrected due to a change in the lead configuration used to measure the noise. The length between the voltage leads was doubled and the normalized noise power has a L_{z}^{-1} dependence. Therefore, the noise

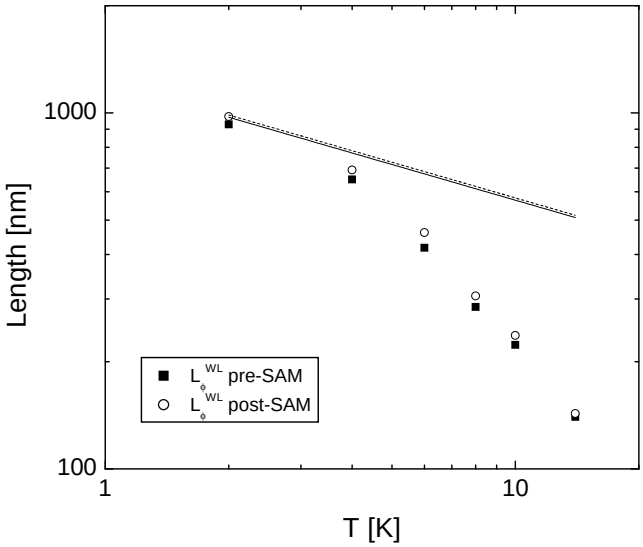

Figure 4.17: L_ϕ^{WL} inferred from a 70 nm wide Au nanowire. The slight changes in the coherence length are most likely due to a slight change in the diffusion length of the Au.

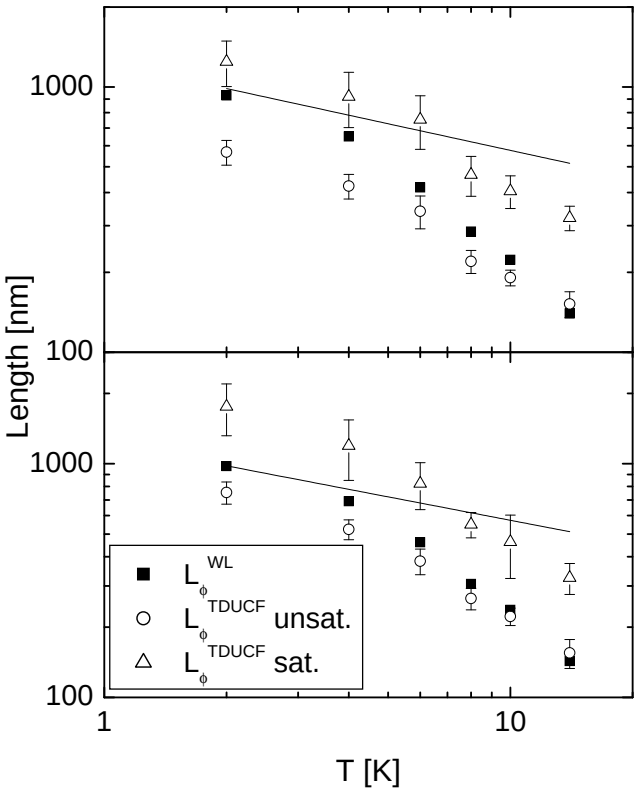

Figure 4.18: The coherence length comparison for an 70 nm wide Au wire before (top) and after (bottom) assembly of a dodecanethiol SAM.

after air exposure was multiplied by 2.

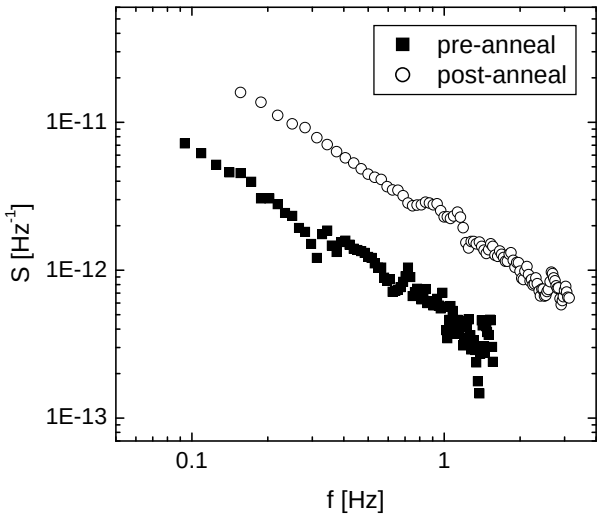

Figure 4.19: The normalized noise power of a 80 nm wide Au wire with a 1.5 nm Ti adhesion layer before and after extended exposure to ambient lab conditions. The noise power after exposure was corrected for a change in the lead configuration.

The change in the noise power cannot be accounted for due to a change in the resistivity (the resistivity dropped by about 20 % due to annealing). The resistivity shows up in two places in the normalized noise power dependence, once simply due to the resistance noise power's dependence on R^4 and the thermal length's dependence on the diffusion constant ($D = 1/\rho e^2 \nu$ where ν is the density of states at the Fermi level). Thus, if correcting for the change in the resistivity, the noise after annealing would need to be increased by 20 % more! The only other parameter the noise power depends on that may have changed while sitting in air is the coherence length and TLS concentration. If anything, the ideas of local interference theory would argue that annealing would lower the TLS concentration. However, the noise power increased meaning that the most probable parameter changed is the coherence length. The fact that L_ϕ^{TDUCF} shows little change between the measurements before and after air exposure is a strong indication that these

values were not correctly inferred from the data, and after annealing the system is in the intermediate regime between saturated and unsaturated.

There is only one other possible explanation for the results of the Ti/Au experiment. For this case, the results of the coherence length comparison between L_ϕ^{WL} and the unsaturated L_ϕ^{TDUCF} are correct. In this explanation, L_ϕ^{WL} and L_ϕ^{TDUCF} are truly different, but depend identically on the spin-flip scattering length. This is why a strong agreement is seen before annealing and not after. However, the change in the noise power needs an explanation. In this scenario, the only way the noise power gets larger after annealing is due to a dramatic increase in the concentration of TLS causing TDUCF. The two acts of annealing and lowering spin-flip scattering do not provide an obvious means for such a TLS concentration change to occur. It would appear that of the two possible ways to interpret the data from this experiment, the explanation that L_ϕ^{TDUCF} has actually changed seems more likely.

The results of the SAM experiment only seem to reinforce the idea that the explanation for the coherence length disagreement observed in Au and Ag is due to improperly using the unsaturated crossover function to fit the TDUCF data. The results clearly show a decrease in the noise power after the SAM assembly. As with the Ti/Au experiment, the noise power change cannot be accounted for due to a resistance change as the sample resistance changed by only $\sim$3 %. The most likely change is a decrease in the number of contributing TLS near the surface of the Au. The SAM molecules could be acting as anchors not allowing impurity motion near the Au surface. This fact combined with the small increase seen in L_ϕ^{TDUCF} after SAM assembly points again to the unsaturated/saturated hypothesis. In this situation, the reduced TLS have lowered the

TDUCF pushing the system farther into the unsaturated regime. When this occurs the unsaturated crossover function should become a better indicator of the true coherence length. Thus, L_ϕ^{TDUCF} should appear to increase.

The other possible explanation for the results of the SAM experiment is the SAM is actually reducing some unknown dephasing rate that only effects TDUCF. At the same time, it is significantly reducing the TLS concentration to account for the fact that an increased L_ϕ^{TDUCF} would result in a larger noise power. Again, the explanation supporting the saturated/unsaturated hypothesis appears to be the more likely scenario.

The last issue to discuss is the MFUCF/TDUCF comparison and what it may imply. For the Au samples with no Ti or SAM, the comparison yielded $\sim$160 decades necessary in order for the integrated TDUCF noise power to equal the MFUCF variance. Again, this is much more than the expected number of 20 if the system was completely saturated. As mentioned earlier, although the samples show no evidence of being completely saturated, the number of decades needed to integrate the TDUCF over to recover the MFUCF variance seem high if the samples are truly approaching the saturated limit. There are two possibilities to explain this observation. One is the comparison itself is flawed due to some missing constant or something of this nature. The other possibility is the noise power does not have a $1/f$ dependence over the bandwidth integrated. In these experiments, the noise power is measured to, at most, 6.25 Hz. To perform the TDUCF/MFUCF comparison, the $1/f$ behavior of the noise is assumed to hold over all frequency space (at least between the limits of the TDUCF integration). If this functional form does not hold and the noise power at higher frequencies is **larger** than expected, then the comparison will always overestimate the number of decades required to recover the MFUCF variance.

This, in turn, would imply that the distribution of TLS is not as flat as assumed. There would need to be a larger number of TLS with short characteristic times in order for this to be possible.

Chapter 5

Conclusion

5.1 Future Work

The experiments detailed in the previous pages attempted to answer one of the two unsolved mysteries of phase coherence physics in normal metals. The apparent disagreement between coherence lengths inferred from weak localization magnetoresistance and the magnetic field dependence of time-dependent universal conductance fluctuations was found to likely be a result of improperly analyzing the conductance fluctuation data. The implication that in clean gold and silver the time-dependent universal conductance fluctuations are approaching the universal limit may be quite profound. When this fact is combined with the comparison of the TDUCF noise power to the MFUCF variance, the results could imply that the distribution of TLS is not as well understood as currently believed.

The importance of two level systems has been renewed due to the recent work with solid-state qubits [46]. It has been suggested that a fundamental limitation of such a qubit is dephasing by $1/f$ type noise [47]. If the TLS distribution question is ubiquitous to all systems, then a larger-than-expected high frequency noise could cause extra dephasing in qubit systems as well. Investigations into the $1/f$ noise at higher frequencies seems to be the most fruitful experimental endeavor with the largest possible impact in the physics community. How to study a high frequency noise that has some type of inverse power law dependence on frequency is a very difficult to answer. As was discovered when attempting

the noise measurements discussed in this thesis, the $1/f$ noise-to-white background noise ratio is not conducive to measuring TDUCF much past 10 Hz. In the saturated limit, the noise power would require integration up to the megahertz level, so the upper limit to current noise measurements would require an enormous improvement.

Assuming that the coherence length disagreement question has been answered, the only major question left in the field of phase coherence in normal metals is, "what causes coherence saturation at low temperatures?" This question has been hotly debated for some time now with two main opinions. One group insists that the saturation is an intrinsic effect while the other insists that extrinsic effects cannot be eliminated well enough to ignore them as the cause. Both camps have very compelling arguments, but no experiment has been able to unequivocally answer the saturation question. The problem with this issue is that to systematically eliminate all possible extrinsic dephasing mechanisms is incredibly time-consuming, and may simply not be possible in any conceivable sample architecture. On the other hand, the only way to argue that some extrinsic mechanism is causing saturation is to create a system with such a mechanism. In this case, a intrinsic saturation mechanism may just be washed out. The Ag results give an example of why eliminating all possible extrinsic causes of saturation is difficult. In the Ag data, no measurements performed were able to identify the presence of magnetic impurities even though a saturation was observed below 1 K. However, since noise measurements were not possible at these low temperatures, a rigorous check for these impurities was not possible. Thus, it was not possible to completely discount magnetic impurities as the cause of the saturation seen in Ag. It maybe necessary to move away from the conventional normal metals and try performing these phase coherence experiments in more controllable

systems such as a 2DEG [48]. There are issues, however, that would need to be overcome including producing a system that is weakly disordered, not ballistic.

5.1.1 Closing Remarks

The bulk of the theory explaining weak localization and universal conductance fluctuations has become excepted fact in the physics community and has held that status for at least 20 years. I believe that weak localization will remain an important tool to investigate phase coherence as devices such as quantum computers remain relevant. However, I believe the experimental tools required to observe WL magnetoresistance will remain important for another reason. Such an experiment is quickly becoming cheap enough to consider as an education tool for physics undergraduates.

Much like when I first had the chance to observe the superconducting transition in my senior lab, I think observing the WL magnetoresistance is an experiment that would teach undergraduates interested in condensed matter physics an incredible number of skills. This experiment can teach the basics of vacuum systems, evaporation techniques, cryogenic techniques, and ac transport methods. Most importantly, the phenomena can be observed in larger systems so samples can be made with a simple shadow mask instead of the electron beam lithography used to produce the samples discussed in this thesis. The basic ideas explaining weak localization are approachable to any student that has taken a quantum mechanics course and introductory electricity and magnetism course. The experiment also would give students a tangible example of quantum mechanics instead of just a particle in a box or a hydrogen atom homework problem.

The TDUCF, however, do not appear to have the same possibilities as WL. As clearly

shown in this thesis, choosing to infer coherence length information from the magnetic field crossover of TDUCF is both extremely time-consuming and possibly very inaccurate. The physical effect is also extremely small making it very difficult to observe in all but the smallest devices. As a tool for investigating phase coherence in any material, TDUCF ranks a distant third behind WL and the Aharonov-Bohm effect. Even the magnetofingerprint (which is much easier to observe), is not very useful since gaining any believable coherence information requires a huge magnetic field range.

As a graduate research project, I believe the past five years have given me an incredible number of experimental skills as well as a honed intuition for transport measurements in mesoscopic systems. If I wish to continue such measurements, though, I will need to find a new system of study. My experiences over the last five years has convinced me that the condensed matter physics community, in general, views this as a "completed" field (and has so for many years). With the apparent answer to one of the two outstanding issues in the field, I must agree. It is no longer a field requiring much investigation. For one, there is little doubt that normal metals would make a horrible system for a qubit; the coherence lengths in systems like 2DEG's and nanotubes can be an order of magnitude larger. It also appears the only question left to answer about the normal metal systems may be too difficult to solve experimentally. However, there has been some interest in exploring electron phase coherence in magnetic materials [49][50]. Also, with single molecule transistors, heterostructure quantum dots, and other novel nanoscale systems left to study, there are still an incredible number of experimental opportunities "at the bottom."

References

[1] D. Hoadley, P. McConville, and N. O. Birge, "Experimental comparison of the phase-breaking lengths in weak localization and universal conductance fluctuations," *Phys. Rev. B*, vol. 60, pp. 5617–5625, 1999.

[2] Y. M. Blanter, "Electron-electron scattering rate in disordered mesoscopic systems," *Phys. Rev. B*, vol. 54, pp. 12807–12819, 1996.

[3] I. L. Aleiner and Y. M. Blanter, "Inelastic scattering time for conductance fluctuations," *Phys. Rev. B*, vol. 65, pp. 115317–115326, 2002.

[4] P. Mohanty, E. M. Q. Jariwala, and R. A. Webb, "Intrinsic decoherence in mesoscopic systems," *Phys. Rev. Lett.*, vol. 78, pp. 3366–3369, 1997.

[5] D. Golubev, A. Zaikin, and G. Schön, "On low-temperature dephasing by electron-electron interaction," *J. Low Temp. Phys.*, vol. 126, pp. 1355–1376, 2002.

[6] B. L. Altshuler, A. G. Aronov, and D. E. Khmelnitsky, "Suppression of localization effects by the frequency field and nyquist noise," *Solid State Commun.*, vol. 39, pp. 619–623, 1981.

[7] F. Pierre and N. O. Birge, "Dephasing by extremely dilute magnetic impurities revealed by aharonov-bohm oscillations," *Phys. Rev. Lett.*, vol. 89, pp. 206804–206807, 2002.

[8] P. Drude, "Zur elektronentheorie der metalle," *Annalen der Physik*, vol. 306, pp. 566–613, 1900.

[9] N. W. Ashcroft and N. D. Mermin, *Solid State Physics*. Saunders College Publishing, 1976.

[10] R. P. Feynman, R. B. Leighton, and M. Sands, *The Feynman Lectures on Physics Volume III*. Addison-Wesley Publishing Company, 1965.

[11] M. E. Gershenson, "Low-temperature dephasing in disordered conductors: experimental aspects," *Annalen der Physik*, vol. 8, pp. 559–568, 1999.

[12] G. Bergmann, "Physical interpretation of weak localization: A time-of-flight experiment with conduction electrons," *Phys. Rev. B*, vol. 28, p. 29142920, 1983.

[13] D. K. Ferry and S. M. Goodnick, *Transport in Nanostructures*. Cambridge University Press, 1997.

[14] V. Chandrasekhar, P. Santhanam, and D. E. Prober, "Effect of spin-orbit and spin-flip scattering on conductance fluctuations," *Phys. Rev. B*, vol. 42, pp. 6823–6826, 1990.

[15] G. Bergmann, "Weak localizations." lecture notes.

[16] G. Bergmann, "Influence of spin-orbit coupling on weak localization," *Phys. Rev. Lett.*, vol. 48, pp. 1046–1049, 1982.

[17] J. S. Moon, N. O. Birge, and B. Golding, "Observation of universal conductance-fluctuation crossovers in mesoscopic Li wires," *Phys. Rev. B*, vol. 56, pp. 15124–15132, 1997.

[18] D. Natelson, R. L. Willett, K. W. West, and L. N. Pfeiffer, "Geometry-dependent dephasing in small metallic wires," *Phys. Rev. Lett.*, vol. 86, pp. 1821–1824, 2001.

[19] F. Pierre, A. B. Gougam, A. Anthore, H. Pothier, D. Esteve, and N. O. Birge, "Dephasing of Electrons in mesoscopic metal wires," *Phys. Rev. B*, vol. 68, pp. 85413–85427, 2003.

[20] M. Aprili, J. Lesueur, L. Dumoulin, and P. Nedellec, "Weak localization and electron-electron interaction in percolating nickel films," *Solid State Commun.*, vol. 102, pp. 41–46, 1997.

[21] B. L. Altshuler, A. G. Aronov, and P. A. Lee, "Interaction effects in disordered Fermi systems in two dimensions," *Phys. Rev. Lett.*, vol. 44, pp. 1288–1291, 1980.

[22] J. B. Johnson, "Thermal agitation of electricity in conductors," *Phys. Rev.*, vol. 32, pp. 97–109, 1928.

[23] H. Nyquist, "Thermal agitation of electric charge in conductors," *Phys. Rev.*, vol. 32, pp. 110–113, 1928.

[24] P. Dutta and P. M. Horn, "Low frequency fluctuations in solids: $1/f$ noise," *Rev. Mod. Phys.*, vol. 53, pp. 497–516, 1981.

[25] B. L. Altshuler, P. A. Lee, and R. A. Webb, eds., *Mesoscopic Penomena in Solids.* North-Holland Press, 1991.

[26] P. J. McConville, *A Quantitative Test of Quantum Transport in Ag Films.* PhD thesis, Michigan State University, 1995.

[27] N. O. Birge, B. Golding, and W. H. Haemmerle, "Electron quantum interference and $1/f$ noise in bismuth," *Phys. Rev. Lett.*, vol. 62, pp. 195–198, 1989.

[28] P. A. Lee, A. D. Stone, and H. Fukuyama, "Universal conductance fluctuations in metals: Effects of finite temperature, interactions, and magnetic field," *Phys. Rev. B*, vol. 35, pp. 1039–1070, 1987.

[29] D. J. Thouless, "Maximum metallic resistance in thin wires," *Phys. Rev. Lett.*, vol. 39, pp. 1167–1169, 1977.

[30] S. Feng, P. A. Lee, and A. D. Stone, "Sensitivity of the conductance of a disordered metal to the motion of a single atom: implications for $1/f$ noise," *Phys. Rev. Lett.*, vol. 56, pp. 1960–1963, 1986.

[31] S. Feng, P. A. Lee, and A. D. Stone, "Erratum: Sensitivity of the conductance of a disordered metal to the motion of a single atom: implications for $1/f$ noise," *Phys. Rev. Lett.*, vol. 56, p. 2772, 1986.

[32] A. D. Stone, "Reduction of low-frequency noise in metals by a magnetic field: Observability of the transition between random-matrix ensembles," *Phys. Rev. B*, vol. 39, pp. 10736–10743, 1989.

[33] B. L. Altshuler, "Variation of the random potential and the conductivity of samples of small dimensions," *JETP lett.*, vol. 42, pp. 447–450, 1985.

[34] P. A. Lee and A. D. Stone, "Universal conductance fluctuations in metals," *Phys. Rev. Lett.*, vol. 55, pp. 1622–1625, 1985.

[35] J. H. Scofield, "ac method for measuring low-frequency resistance fluctuation spectra," *Rev. Sci. Instr.*, vol. 58, pp. 985–993, 1987.

[36] A. Trionfi, S. Lee, and D. Natelson, "Electronic coherence in metals: comparing weak localization and time-dependent conductance fluctuations," *Phys. Rev. B*, vol. 70, pp. 041304–041307, 2004.

[37] J. J. Lin and N. Giordano, "Electron scattering times from weak localization studies of au-pd films," *Phys. Rev. B*, vol. 35, pp. 1071–1075, 1987.

[38] I. L. Aleiner, "The formulas for the fits." private communication.

[39] C. W. J. Beenakker and H. van Houten, "Flux-cancellation effect on narrow-channel magnetoresistance fluctuations," *Phys. Rev. B*, vol. 37, pp. 6544–6546, 1988.

[40] J. V. C. Van Haesendonck and Y. Bruynseraede, "Resonant kondo scattering of weakly localized electrons," *Phys. Rev. Lett.*, vol. 58, pp. 1968–1971, 1987.

[41] J. Wei, S. Pereverzev, and M. E. Gershenson, "Microwave-induced dephasing in one-dimensional metal wires," *Phys. Rev. Lett.*, vol. 96, pp. 086801–086804, 2006.

[42] A. Trionfi, S. Lee, and D. Natelson, "Time-dependent universal conductance fluctuations and coherence in aupd and ag," *Phys. Rev. B*, vol. 72, pp. 035407–035416, 2005.

[43] Z. Ovadyahu, "Nonequilibrium dephasing in two-dimensional indium oxide films," *Phys. Rev. B*, vol. 63, pp. 235403–235416, 2001.

[44] G. Bergmann, "Weak localization as a tool to investigate magnetic properties," *J. of Magnetism and Magnetic Materials*, vol. 54-57, pp. 1433–1436, 1986.

[45] L. H. Yu, Z. K. Keane, J. W. Ciszek, L. Cheng, J. M. Tour, T. Baruah, M. R. Pederson, and D. Natelson, "Kondo resonances and anomalous gate dependence in the electrical conductivity of single-molecule transistors," *Phys. Rev. Lett.*, vol. 95, pp. 256803–256806, 2005.

[46] Y. Nakamura, Y. A. Pashkin, T. Yamamoto, and J. S. Tsai, "Charge echo in a cooper-pair box," *Phys. Rev. Lett.*, vol. 88, pp. 047901–047904, 2002.

[47] J. Schriefl, M. Clusel, D. Carpentier, and P. Degiovanni, "Nonstationary dephasing of two-level systems," *Europhys. Lett.*, vol. 69, pp. 156–162, 2005.

[48] J. A. Katine, M. J. Berry, R. M. Westervelt, and A. C. Gossard, "Determination of the electronic phase coherence time in one-dimensional channels," *Phys. Rev. B*, vol. 57, pp. 1698–1702, 1998.

[49] G. Tatara, H. Kohno, E. Bonet, and B. Barbara, "Aharonov-bohm oscillation in a ferromagnetic ring," *Phys. Rev. B*, vol. 69, pp. 054420–054424, 2004.

[50] S. Lee, A. Trionfi, and D. Natelson, "Quantum coherence in a ferromagnetic metal: time-dependent conductance fluctuations," *Phys. Rev. B*, vol. 70, pp. 212407–212410, 2004.

[51] G. Bergmann, "Weak localization in thin films: a time-of-flight experiment with conduction electrons," *Phys. Rep.*, vol. 107, pp. 1–58, 1984.

[52] G. Bergmann and H. Beckmann, "Identification of local spin fluctuations by weak localization," *Phys. Rev. B*, vol. 52, pp. R15687–R15690, 1995.

[53] B. W. Gardner, J. C. Wynn, P. G. Björnsson, E. W. J. Straver, K. A. Moler, J. R. Kirtley, and M. B. Ketchen, "Scanning superconducting quantum interference device susceptometry," *Rev. Sci. Inst.*, vol. 72, pp. 2361–2364, 2001.

Appendix A

Nonlinear Fitting in Mathematica

All of the coherence length data reported in this thesis was inferred from data fit using the nonlinear fitting command in Mathematica. This appendix will discuss the basic procedure to perform such a fit and what the confidence intervals represent.

The first step in performing a non-linear fit in mathematica is to define the functional form of the fit. To do this properly, the function must be defined in this way:

```
fitfun[x_ ]:= desired fitting function
```

By placing the underscore after the variable x, any variable or number can be used in place of x. The colon before the equals sign is also necessary for the function to be defined properly. Typically, there were many constants in each fitting function that were sample dependent. For this reason, I made one input for sample parameters including things like sample resistance, width, length, and diffusion constant.

An example of the initial function and parameter inputs for a typical weak localization magnetoresistance fit are shown below.

$$\texttt{Lh[B\_]:=}\sqrt{\frac{\hbar}{eB}}$$

$$\texttt{rk = }\frac{h}{e^2}$$

$$\texttt{B}\phi\texttt{ = }\frac{\hbar}{4eL\phi^2}$$

$$\texttt{fit1D[B\_]:=}\frac{2r}{rkL}\left(\frac{3}{2}\left(\frac{1}{L\phi^2}+\frac{4}{3Lso^2}+\frac{1}{3}\left(\frac{w}{Lh[B]}\right)^2\right)^{-1/2}-\frac{1}{2}\left(\frac{1}{L\phi^2}+\frac{1}{3}\left(\frac{w}{Lh[B]}\right)^2\right)^{-1/2}\right)$$

```
r = 3530
e = 1.602*^-19
h = 6.626*^-34
ħ = h/2/Pi
w = 125*^-9

L = 41*^-6
```

Once the parameters and fitting function are input into the mathematica kernel, the only other information needed is the data that will be fit. The easiest way to do this is to sort the magnetoresistance data in excel and then save the resultant curves as .txt files. Once this is done, the data can be imported to mathematica. This is done in the following manner:

```
data = Import["File path","Table"]
```

If the data was saved correctly as a .txt file, then "data" should now be a two column array. All the necessary information has now been input into the kernel. All that is left is to fit the data.

The first step in the fitting procedure is to load the nonlinear fit package. This is done by inputting:

```
<< Statistics`NonlinearFit`
```

Once this package is loaded into the kernel, the"NonlinearFit" command may be used. The command is used in the following way:

```
fitfun = NonlinearFit[data,fit1D[B],B,{{Lso,300*^-9},{Lϕ,300*^-9}}]
```

The values in the curly brackets are initial guesses of each free parameter in the fitting function. If these guesses are not made, the fitting command will not work. The output of this command is the functional form of the fitting function. The best fit is determined by standard χ^2 analysis. Unfortunately, the fitting parameters are not distinguishable in the output. In order to quickly output the values of the fitting parameters, the following command is used:

```
BestFitParameters/.NonlinearRegress[data,fit1D[B],B,{{Lso,300*^-9},
{Lϕ,300*^-9}},RegressionReport->BestFitParameters]
```

The output of this command will give only the best fit value of any free parameter in the fitting function.

The "NonlinearRegress" command will calculate many other parameters involved in the fitting. The only other physically significant values are the confidence intervals. In the output of the command, the confidence intervals are labeled CI. These values are based on a 95 % confidence level. The details of how the confidence intervals are truly calculated are best left for a statistics course, but the method, including the confidence level, is standard. A 95 % confidence level can be thought of as stipulating that if the data set was remeasured many times, then 95 % of the resultant data sets would contain the best fit value reported (within the given confidence intervals).

Appendix B

Anomalous Magnetic Behavior of Ti

It was suggested as early as 1984 [51] that the WL magnetoresistance could be used as a probe of magnetic scattering. It has been shown experimentally that magnetic impurity concentrations down to a few parts per million cause observable changes in many of the quantum transport phenomena [44, 7]. QTPs should provide an excellent tool to probe even extremely dilute magnetic impurity concentrations.

As mentioned in chapter 4, an anomalous magnetic impurity signature attributed to the Ti adhesion layer was employed to alter the coherence physics of the Au nanowires. The work discussed in this appendix attempts to explain the cause of this unexpected behavior. WL measurements on Au and Ag with Ti underlayers were both used to probe the magnetic effect. The results indicate that oxygen vacancies in the Ti oxide are the cause of this behavior. The results also demonstrate the quantitative power of using quantum transport phenomena as a magnetic impurity probe.

The initial Ti test is discussed in chapter 4. Along with this test a more detailed test was performed to observe how the coherence length changed when left near room temperature with some small partial pressure of oxygen present. To perform this test, a 70 nm Au sample was prepared with a 1.5 nm thick Ti adhesion layer. The sample was immediately placed in the cryostat a cooled to 2 K. The WL magnetoresistance was then measured at 2, 4, 6, 8, 10, and 14 K. The sample was then warmed to 305 K and left in vacuum ($\sim$5 Torr) for 24 hours. The sample was cooled down and the WL measurements

were repeated. These process was then repeated once more to observe the change after another 24 hours. The results are shown in Figure B.1

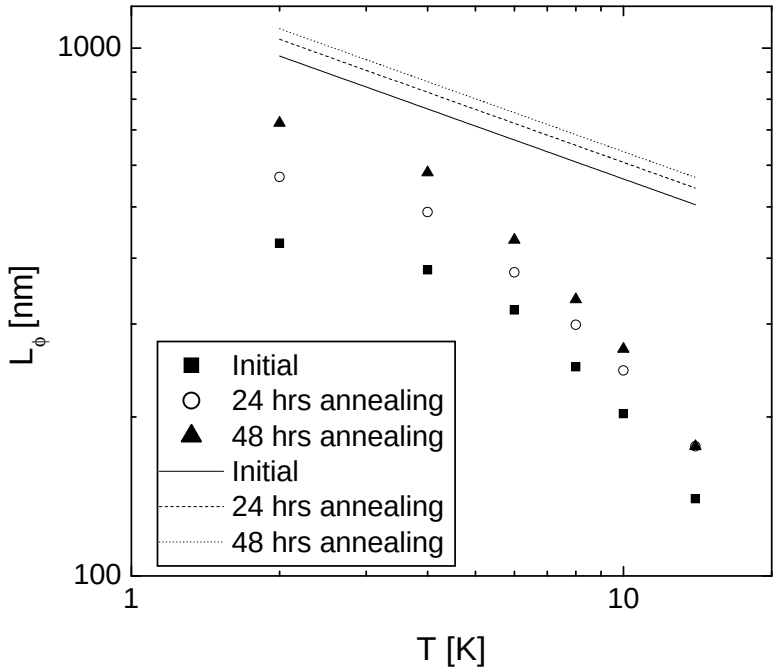

Figure B.1: Coherence lengths of a 70 nm wide Au nanowire with a 1.5 nm thick Ti adhesion layer. The coherence lengths were measured once within an hour of fabrication and then after annealing in 5 Torr for 24 hours and again after 48 hours. The lines are the predicted Nyquist scattering length based on the sample characteristics.

Another important value to examine is the estimated magnetic impurity concentration. The coherence length information before annealing should allow for a quantitative examination of the magnetic impurity concentration since it shows a coherence saturation. For the result shown in Figure 4.15, the coherence length looks nearly saturated at 2 K. Using this value and the Nagaoka-Suhl formula, the magnetic impurity concentration for this sample is about 16 ppm. This number is much higher than the expected total impurity concentration of the source gold (1 ppm). In fact, the number is higher than

the total impurity concentration of the source Ti as measured via spectrographic analysis (∼8 ppm). Assuming the impurities are at the Ti/Au interface, an estimate of the surface density of impurities at the interface gives 14000 impurities/μm^2. SQUID measurements used to observe this small a magnetic signal were unsuccessful. ESR measurements were also attempted, with no apparent magnetic signature.

The second test performed was an examination of the coherence length suppression as a function of the Ti evaporation rate was performed. With the chamber vacuum near 7.5×10^{-7} Torr when the Ti evaporation begins and with titanium's affinity for oxygen, it seems reasonable that the majority of the Ti adhesion layer is actually an oxide by the time the Ag or Au is deposited over it. By adjusting the evaporation rate of the Ti, the stoichiometry of the oxide should change. Observing how suppressed the WL magnetoresistance is as a function of the Ti evaporation rate could indicate whether the oxygen content in the Ti oxide is the cause of the magnetic scattering.

Table B.1 shows the results of the test at the lowest temperature measured, 2 K. Since both the coherence length and coherence time are dependent on the diffusion constant of the metal, it is a little tricky to properly compare coherence information from different samples. In order to avoid this problem, we compared the ratio of the measured coherence time to the expected Nyquist scattering time based on sample characteristics.

There is a clear correlation between the Ti evaporation rate and the coherence suppression at 2 K. The result certainly supports the hypothesis that the magnetic signature seen in samples with a Ti adhesion layer is somehow related to the oxygen content in the Ti oxide.

It is important to mention that there was a similar experiment performed with Ti in

Table B.1: Au and silver samples prepared with a Ti adhesion layer deposited at different rates. The ratio of the measured coherence time to the expected Nyquist scattering time is shown at 2 K.

Material	Ti rate [Å/s]	$\tau_\phi/\tau_{\text{e-e}}$
Ag	-	.82
Ag	.5	.36
Ag	1.5	.14
Au	-	1.14
Au	.3	.71
Au	1	.19

1995 [52] with an observed suppression of the weak localization magnetoresistance. However, in this experiment small fractions of a monolayer of Ti (hundreths of a monolayer) were used and the proposed coherence suppression mechanism was local spin fluctuations. In this case, the extra dephasing rate was roughly proportional to T. In other words, it cannot explain the saturation observed in the initial Au test. For this reason, local spin fluctuations are most likely not the cause of the coherence suppression.

Although typical SQUID measurements yielded no useful information about the Ti/Au system, scanning SQUID microscopy [53] may have more success in determining the cause of this magnetic signature.